SOME EFFECTS OF FORWARD SPEED ON THE PERFORMANCE OF AIR CUSHION VEHICLES

Grumman

RESEARCH DEPARTMENT

MEMORANDUM RM-218

NOVEMBER 1962

GRUMMAN AIRCRAFT ENGINEERING CORPORATION
BETHPAGE, NEW YORK

Grumman Research Department Memorandum RM-218

SOME EFFECTS OF FORWARD SPEED ON THE PERFORMANCE OF AIR CUSHION VEHICLES

by

J. O. Helgesen
Special Projects Section

November 1962

Approved by: Charles E. Mack, Jr.
Charles E. Mack, Jr.
Director of Research

FOREWORD

The wind tunnel data discussed in this report were obtained as part of a study of Supplementary Lift for Air Cushioned Vehicles for the U.S. Army Transportation Research Command (USATRECOM) under Contract DA 44-177-TC-708. The results of the contract study are included in TCREC 62-50 (Vol. II - Data Analysis) and TCREC 62-51 (Vol. III - Performance Analysis). Volume I - Basic Data Report is available from USATRECOM on a loan basis only.

The author would like to acknowledge the aid of Mr. Norman K. Walker, whose ideas form the basis for the data correlation method presented herein, and to Miss Ellen Jungclaus, who patiently waded through the reams of data to plot the graphs presented in this report.

SUMMARY

This report discusses some effects of forward speed on air cushion vehicle performance. It is shown that at a given forward velocity (dependent on height and mass flow) the forward jet is blown rearward. At higher velocities considerable performance improvement could be attained by turning off this jet.

The force and moment data are found to correlate very well with the ratio q_o/q_c, $(\rho V_o ah/2\dot{m})^2$.

TABLE OF CONTENTS

LIST OF ILLUSTRATIONS

LIST OF SYMBOLS

a	width of base (2 ft), includes jet
b	length of base (4 ft), includes jet
C_D	drag coefficient, $\frac{\text{Drag}}{q_o S_b}$
C_L	lift coefficient, $\frac{\text{Lift}}{q_o S_b}$
C_M	pitching moment coefficient $\frac{\text{Pitching Moment}}{q_o S_b b}$, positive nose up.
$C_{D_{mom}}$	momentum drag coefficient $\frac{\dot{m} V_o}{q_o S_b}$
C_j	length of peripheral jet (8 ft)
C_μ	jet momentum coefficient $\frac{\dot{m} V_j}{q_o S_b}$
h	height, measured to base of model
K	constant
$\dot{m}$	mass flow in slugs/sec
p_t	total pressure of peripheral jet above ambient
q_o	free stream dynamic pressure
q_c	dynamic pressure at "critical velocity"
S_b	base area (8 ft^2) includes jet
t_j	jet thickness

V_o	free stream velocity
V_c	"critical velocity"
V_j	mean jet velocity
β	free stream cushion force parameter
θ_j	jet angle, measured from vertical, positive inward
ρ	density of air

Subscripts for Lift, Drag, and Pitching Moment Coefficients

BG	simulated jet attached to ground
BM	simulated jet attached to the model
o	basic model in ground effect, but no jet blowing

INTRODUCTION

In February 1961, the Grumman Research Department initiated a study for the U.S. Army Transportation Research Command (USATRECOM) on Supplementary Lift for Air Cushioned Vehicles (Contract No. DA 44-177-TC-708). During this study (Refs. 1, 2, and 3) wind tunnel tests were conducted on a three-dimensional, half span, reflection plane model (Fig. 1) with an 18 per cent thick modified Clark Y profile. Air supply for the peripheral jets was piped up through the tunnel floor. The leading and trailing edges were removable (Fig. 2) in order to be able to vary the jet configuration readily by replacing the nozzle blocks. When these nozzle blocks were utilized, the wing-chord to ground-effect-base chord varied (in relation to the basic configuration) with jet deflection angle, but not with jet thickness. The ground effect base area varied because of this procedure (-2.3% for $\theta_j = 30°$, +2.7% for $\theta_j = -30°$). The height size parameter for the various configurations and heights discussed in this report are tabulated on the following page.

One particularly annoying factor in the data analysis was the apparent scatter of the drag and moment data when plotted versus the standard jet momentum coefficient C_μ. (The lift data correlated well with C_μ.) This apparent scatter was attributed to the tares in the ducting system and the variation of jet flow distribution with forward speed. It is the purpose of this report to rectify that assertion and present the drag and moment data for the symmetrical jet configurations. It is apparent now that the scatter in the data was not due to the test setup (true - that contributed somewhat), but to the fact that the data are not a function of C_μ, but a function of

$$q_o/q_c = \left(\frac{\rho V_o a h}{2\dot{m}}\right)^2 .$$

The development of this parameter, originally proposed by N. K. Walker (Ref. 4), is discussed in a later section of this report.

h	Configuration t_j/θ_j	$hC_j/4S_b$
2.5	.94/0	.052
	.94/30	.0532
	.94/-30	.0506
	.47/0	.052
	1.41/0	.052
5.0	.94/0	.104
	.94/30	.1064
	.94/-30	.1012
	.47/0	.104
	1.41/0	.104
7.5	.94/0	.156
	.94/30	.1596
	.94/-30	.1518
	.47/0	.156
	1.41/0	.156

This report mainly analyzes the model configurations with symmetrical leading and trailing edge jet nozzles. The force data are presented in coefficient form as a function of the above parameter. Pressure data, taken along the base of the model, are also presented in order to clarify or illustrate what happens to the air cushion as speed increases.

DISCUSSION

Reference 2 discusses the geometric characteristics of the model used during the wind tunnel study of supplemental lift for air cushioned vehicles. The smooth-airfoil shaped model was chosen in order to eliminate some aerodynamic variables and facilitate evaluation of the wind tunnel data. Two types of tests were conducted with the air supply system turned off and (when applicable) the peripheral jet nozzles taped shut.

The first of these tests determined the basic aerodynamic characteristics of the model at zero angle of attack in proximity to the ground. For these tests the peripheral jets were taped shut to present a smooth undersurface. Data from these tests are tabulated below.

h	C_{L_o}	C_{D_o}	C_{m_o}
2.5	.1147	.0441	.0329
5.0	.0761	.0377	.0294
7.5	.0671	.0403	.0224

Additional aerodynamic data, with the model at various angles of attack, were gathered in a later portion of this test series, but these are not of interest for this report.

The second set of tests evaluated the aerodynamic characteristics of the model with a simulated jet. These are called "mound flow" tests. The jet curvature, or shape, of the ACV in the hovering mode was replicated with solid material. Two conditions were evaluated. One of these conditions had the simulated jet attached to the model while the other had the jet attached to the ground. (In the former condition, forces acting on the simulated jet are transmitted to the model, while in the latter tests they are not.) The data from these tests are tabulated on the following page.

h	$C_{L_{BG}}$	$C_{D_{BG}}$	$C_{m_{BG}}$	$C_{L_{BM}}$	$C_{D_{BM}}$	$C_{m_{BM}}$
2.5	.41	.024	.05	.43	.067	.046
5.0	.58	.045	.065	.58	.105	.055
7.5		.0761*		.691*	.1435*	

*Estimated, see Appendix.

The data tabulated for the 7.5-inch height were estimated on the basis of data at the lower heights. The estimation procedure is discussed in the Appendix.

Development of Correlation Parameter

The first tests at Grumman on the forward speed characteristics of Air Cushion Vehicles were conducted during 1959, Ref. 5. At the time of testing, we were more interested in the effect of forward speed on the jet than in the effect of planform on the forward speed characteristics. As a result, the model tested was a quasi-two-dimensional representation of an annular jet, and represents the stagnation point in a three-dimensional model. It was determined at that time that there was a direct relationship between the $\Delta P_b/q_{j_o}$ ratio that had correlated the two-dimensional hovering data ($\Delta P_b/q_{j_o}$ is a function of jet geometry and height only) and the ratio $q_o/\Delta P_b$ (free stream dynamic head divided by base pressure). The results of these tests indicated that the forward jet remains intact until the dynamic head due to forward speed is slightly greater than the base pressure; thereafter there is an approximately linear increase in base pressure with forward speed dynamic head. However, these tests represented the jet stagnation point, and did not include the effects of planform shape.

Two particular factors discouraged us from using this as a correlation parameter in our work. First of all, the results of our pressure data indicated a strong variation of base pressure distribution with forward speed. Second, since our jets were fed from a common source, the jet flow distribution also varied with

forward speed. This latter factor was given in Ref. 2 as one of the reasons for our apparent scatter when attempting to correlate the drag data with jet momentum coefficient C_μ.

Mr. Norman K. Walker, ACV consultant to USATRECOM and ONR, has recently proposed a new parameter for correlating the force data from ACV wind tunnel tests, and for use in predicting the forces acting on an ACV at forward speed. This was first discussed during one of our personal contacts, and later at the IAS-NAVY National Meeting on Hydrofoils and Air Cushion Vehicles (Ref. 4). In particular, the velocity at which the external flow begins to pass below the base is defined as the "second critical velocity." (A premature transition can occur first when $q_o = p_t$, if h is small.) This second critical velocity is calculated to be

$$V_c = \left(\frac{2\dot{m}}{\rho h a}\right)\left(\frac{K}{C_D}\right) = \frac{2\dot{m}}{\rho h a}$$

if K/C_D is chosen as 1.0. (Actually, according to Mr. Walker, K decreases with height, see Ref. 4.)

The ratio of free stream dynamic head to the dynamic pressure of the second critical velocity is then

$$\frac{q_o}{q_c} = \left(\frac{\rho V_o h a}{2\dot{m}}\right)^2 .$$

When q_o/q_c equals 1.0, the mass flow of air attempting to enter the cushion due to free stream equals twice mass flow of air encompassing the cushion from the jets.

Although we are not completely satisfied with the derivation of this parameter, the results presented in Ref. 4 and our own results (discussed in the next section) certainly verify the selection of the variables in q_o/q_c as a correlation parameter for ACV wind tunnel test results.

Force Data

Figures 3 through 7 present various forms of the force data (lift, drag, and pitching moment coefficients) as functions of q_o/q_c. For each jet configuration, three values of mass flow at each of three velocities (nine combinations) were tested. The force data correlation is excellent.

The variation of $C_L - C_{Lo}$ with q_o/q_c for three jet angles is presented in Fig. 3. The effect of jet angle is seen to be most predominant at the lower values of q_o/q_c. The mound flow data presented on these curves are the jet simulation results with the simulated jet attached to the model. The mound flow value of $C_L - C_{Lo}$ is approximately equal to the total model C_L at q_o/q_c equal to 1.0. Multiplying C_L by q_o/q_c and plotting versus q_o/q_c produces an interesting result, Fig. 4. First of all, the effect of jet angle is more distinguishable, even at the 7.5-inches height. It can also be seen, that at q_o/q_c less than 1.0, the slope of the $C_L q_o/q_c$ curve is approximately equal that of the mound flow data (range of q_o/q_c depends on height). At q_o/q_c greater than 1.0, the slope of the $C_L q_o/q_c$ gradually decreases, and should equal that for the basic model at very high q_o/q_c.

The variation of $C_D - C_{Do}$ with q_o/q_c is presented in Fig. 5. These data are very encouraging since, when we plotted this same data versus C_μ, there seemed to be excessive scatter. The mound flow data (simulated jet attached to the model) are also shown on this plot. There are, however, some discrepancies between these data and the results of Ref. 4. Our drag does not peak (and equal mound flow drag at the peak) at q_o/q_c equal to 1.0, and then decrease proportional to $1/V_o$. Instead, our results increase with q_o/q_c and are approximately constant at large q_o/q_c.

The parameter $(C_D - C_{Do})/C_{Dmom}$, suggested in Ref. 4 has been presented in Fig. 6, using our data. C_{Dmom} is the theoretical momentum drag coefficient.

$$C_{Dmom} = \frac{\dot{m}V_o}{q_o S_b}$$

Again, our results are in a form similar to that presented in Ref. 4, but the scatter among $(C_D - C_{Do})/C_{Dmom}$ is considerably greater than when C_{Dmom} is omitted.

The last of the force data, the variation of $(C_m - C_{mo})$ with q_o/q_c, is presented in Fig. 7. For each height, all the force data fall on one pair of curves. There is a consistent discontinuity in curves presented. The values of q_o/q_c, for which this discontinuity occurs, are tabulated below.

h	q_o/q_c
2.5	.105
5.0	.4
7.5	.75

It is at these values of q_o/q_c that a significant variation of flow pattern occurs. The base pressure data also indicate this.

Pressure Data

Base pressure distribution at four spanwise locations are presented in Figs. 8 through 24 for various configurations and heights. The data do confirm the basic change in flow pattern at specific values of q_o/q_c, as indicated previously.

Figures 8 through 10 present base pressure distribution at 7.5-inches height. There is a continual change in pressures (both magnitude and distribution) as q_o/q_c increases, but a radical change takes place between q_o/q_c of 0.5 and 0.8.

Figure 11 shows this change occurring at q_o/q_c between 0.3 and 0.4 for h = 5.0 inches. If the leading edge jet is turned off, however, this radical decrease in base pressure at forward portion of the base does not occur, Figs. 12 through 14. Actually therefore, the leading edge jet at these values of

q_o/q_c (and above) is detrimental. Not only would you waste power (25 per cent for this configuration) by keeping the leading edge jet on unnecessarily, but you would suffer a loss in lift as well.

Base pressure data obtained for these same configurations at 2.5-inch height also verify this, Figs. 15 through 24. The pressure data indicate that, at this height, the change in flow pattern occurs at values of q_o/q_c slightly greater than 0.10. (This was also indicated by the pitching moment data.) For q_o/q_c greater than 0.1, there is a decrease in base pressure at the forward parts of the base as q_o/q_c is increased further. This is illustrated in Figs. 15 through 21. However, if we turn the leading edge jet off, as illustrated in Figs. 22 through 24, there is a continual increase in base pressure as q_o/q_c increases.

REFERENCES

1. Ledesma, R.R., Supplementary Lift for Air Cushioned Vehicles, Volume I of III. Data Report, Aerodynamic Section, Grumman Aircraft Engineering Corporation for U.S. Army Transportation Research Command, Contract DA 44-177-TC-708.

2. Kirschbaum, N., and Helgesen, J., Supplementary Lift for Air Cushioned Vehicles, Volume II of III. Data Analysis, U.S. Army Transportation Research Command, TCREC Technical Report 62-50, June 1962.

3. Kirschbaum, N., and Helgesen, J., Supplementary Lift for Air Cushioned Vehicles, Volume III of III. Performance Analysis, U.S. Army Transportation Research Command, TCREC Technical Report 62-51, June 1962.

4. Walker, N.K., Some Notes on the Lift and Drag of Ground Effect Machines, presented at the IAS-NAVY National Meeting on Hydrofoils and Air Cushion Vehicles, Washington D.C., September 19-20, 1962.

5. Tucker, J.T., Two Dimensional Study of a Low Pressure Annular Jet Ground Effect Machine at Forward Speed, Grumman Research Department Memorandum RM-165, October 1959.

6. Rosenberg, M.R., and Fuller, F.L., Ejector Powered Recirculation Lift Systems for Air Cushion Vehicles, Grumman Research Department Memorandum RM-202, April 1962.

7. Jones, R.S., Some Design Problems of Hovercraft, IAS Paper No. 61-45, presented at the IAS 29th Annual Meeting, New York, New York, January 23-25, 1961.

APPENDIX

ESTIMATE OF MOUND FLOW DATA 7.5-INCH HEIGHT

This discussion of the estimating procedure for mound flow data (in particular lift and drag) at 7.5-inch height is presented here mainly because of one associated parameter, developed along with the estimate. This parameter, β, could be very beneficial in an analytical investigation of ACV lift and drag.

Two types of mound flow tests were conducted. In the one type, the simulated cushion was attached to the model and in proximity to (but not touching) the ground. As a consequence, forces acting on the simulated cushion are transmitted to the model. The force coefficients in this case are subscripted BM. In the other type, the simulated cushion was attached to the ground and in proximity to (but not touching) the model. The force coefficients in this case are subscripted BG. These coefficients have been tabulated on page 5.

For both types of mound flow tests, the flow pattern around the model should be identical. This is illustrated below.

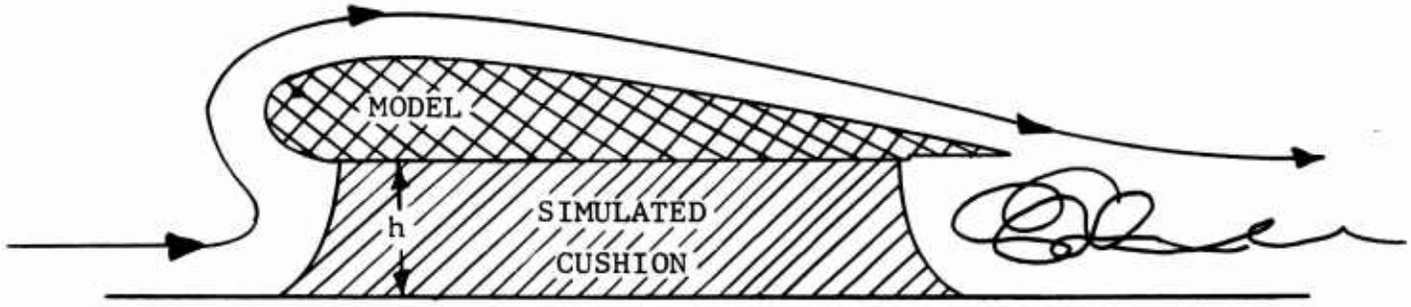

In general, we would expect the drag forces acting on the simulated cushion to be a function of the free stream momentum. We write this as,

$$D_{\substack{\text{Sim} \\ \text{Cush}}} = \beta' \rho V_o^2 ah = \beta q_o ah \qquad (1)$$

β depends on height and planform shape. Rewriting in coefficient form, we find

$$C_{D_{\substack{\text{Sim}\\\text{Cush}}}} = \beta \frac{(ah)}{S_b}$$

We can then calculate β from the data obtained at 2.5-and 5.0-inches height. This is tabulated below.

h	$\frac{ah}{S_b}$	$C_{D_{BM}}$	$C_{D_{BG}}$	β
2.5	.05208	.067	.024	.8143
5.0	.1042	.105	.045	.5758

Figure 25 presents a plot of $C_{D_{BM}}$, $C_{D_{BG}}$, β, and $\frac{1}{2}C_{D_o}$ versus height. The data points are shown with symbols, and solid lines connect these points. Dashed lines are used to show the extrapolation. First of all, we require that

$$C_{D_{BM}} = C_{D_{BG}} = \tfrac{1}{2}C_{D_o} \quad \text{at} \quad h = 0$$

This intersection point is found by a straight line extrapolation of $C_{D_{BM}}$ from $h = 5.0$ and 2.5 inches to $h = 0$, and a continuation of the curve passing through the three given $\frac{1}{2}C_{D_o}$ points. Secondly, examination of Eq. (1) indicates that it is reasonable to require $\beta' = 1.0$ at $h = 0$. This results in $\beta = 2$ at $h = 0$. The equation

$$\beta = 2e^{-.56h^{\frac{1}{2}}} \tag{2}$$

fits the data points at $h = 0$, 2.5, and 5.0. From Eq. (2), $\beta = 0.4312$ at $h = 7.5$ inches. Continuation of the straight line extrapolation for $C_{D_{BM}}$ results in $C_{D_{BM}} = 0.1435$ at $h = 7.5$ inches. Consequently,

$$C_{D_{BG}} = C_{D_{BM}} - \beta \frac{ah}{S_b} = .0761 ,$$

at 7.5-inches height.

Comparison of the two types of mound flow data for lift indicate that the forces acting on the simulated air cushion do not contribute to lift. We do, however, require that at $h = 0$ $C_{L_{BM}} = C_{L_o}$. C_{L_o} at $h = 0$ is found by extending the curve passing through the three given C_{L_o} points. $C_{L_{BM}}$ at 7.5 inches is found by extending the curve passing through the given data at 5.0 and 2.5 inches, and the value of C_{L_o} at $h = 0$. This is illustrated in Fig. 26.

Fig. 1 Photograph of Model in Wind Tunnel

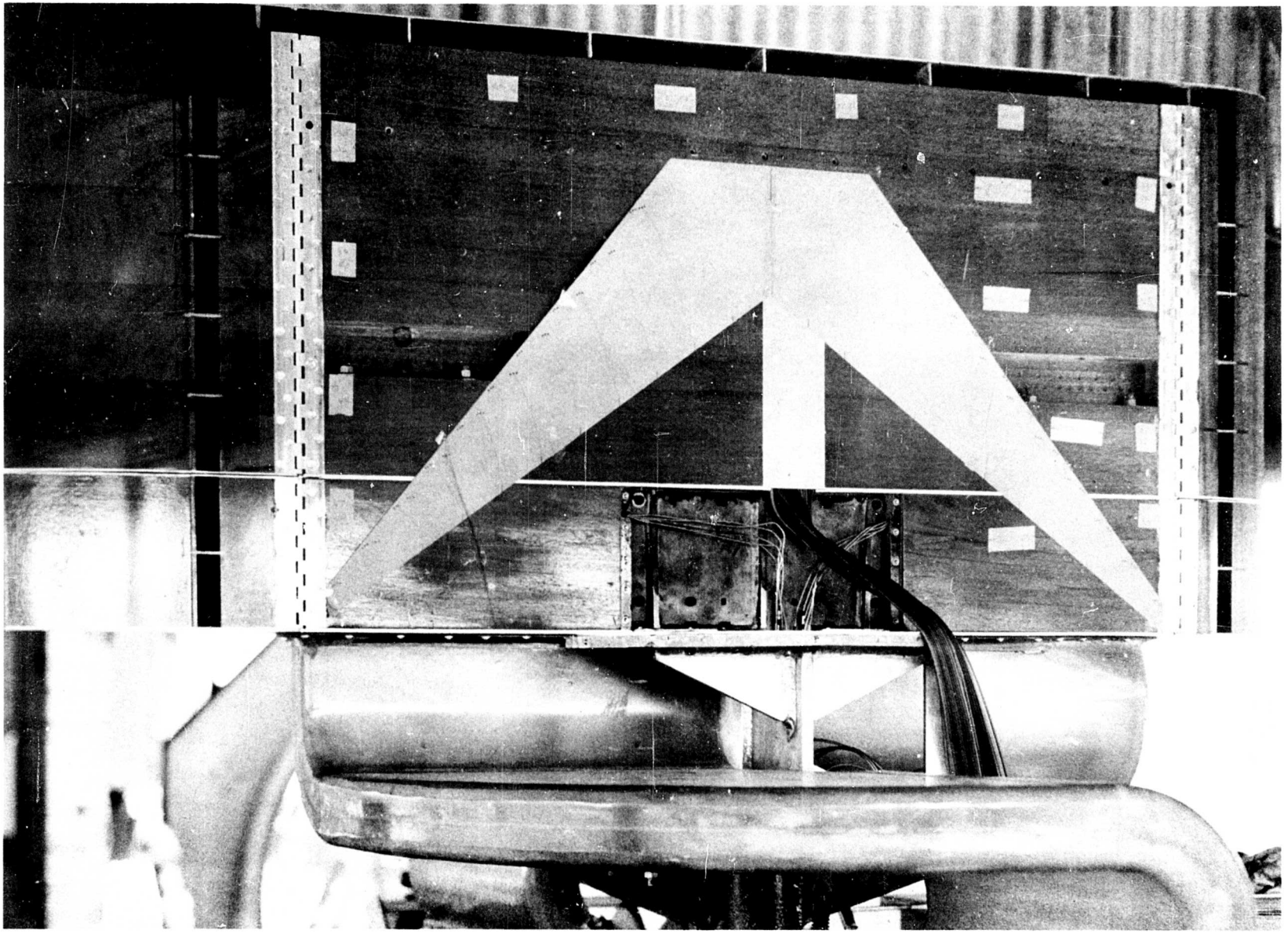

Fig. 2 Photograph of Model Showing Replaceable Leading and Trailing Edge Nozzles

Research Department
RM-218
November 1962

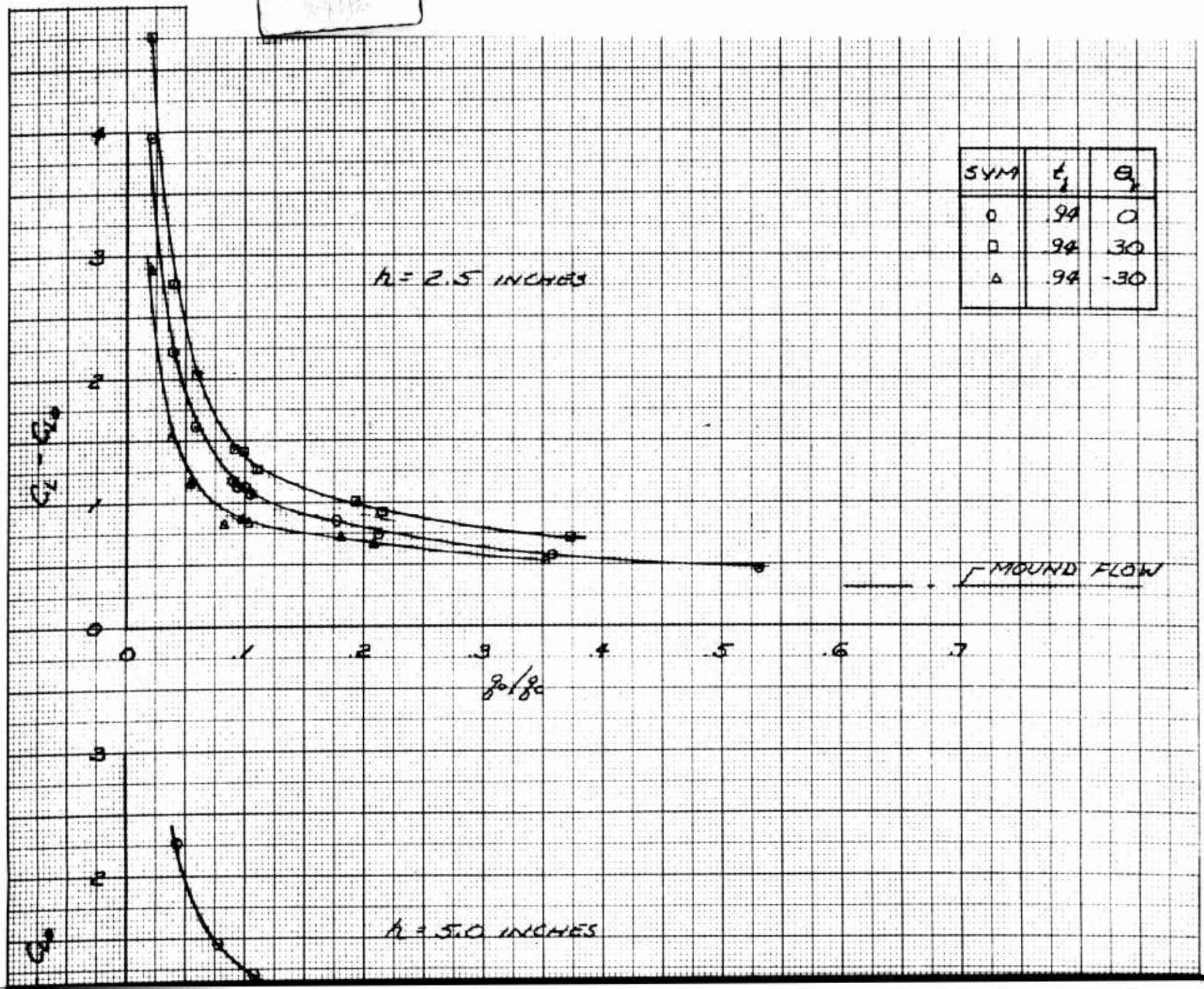
h = 2.5 INCHES
SYM
t_1
θ_1
.94
0
.94
30
.94
-30
MOUND FLOW
C_L
δ_0/δ_c
0
.1
.2
.3
.4
.5
.6
.7
h = 5.0 INCHES

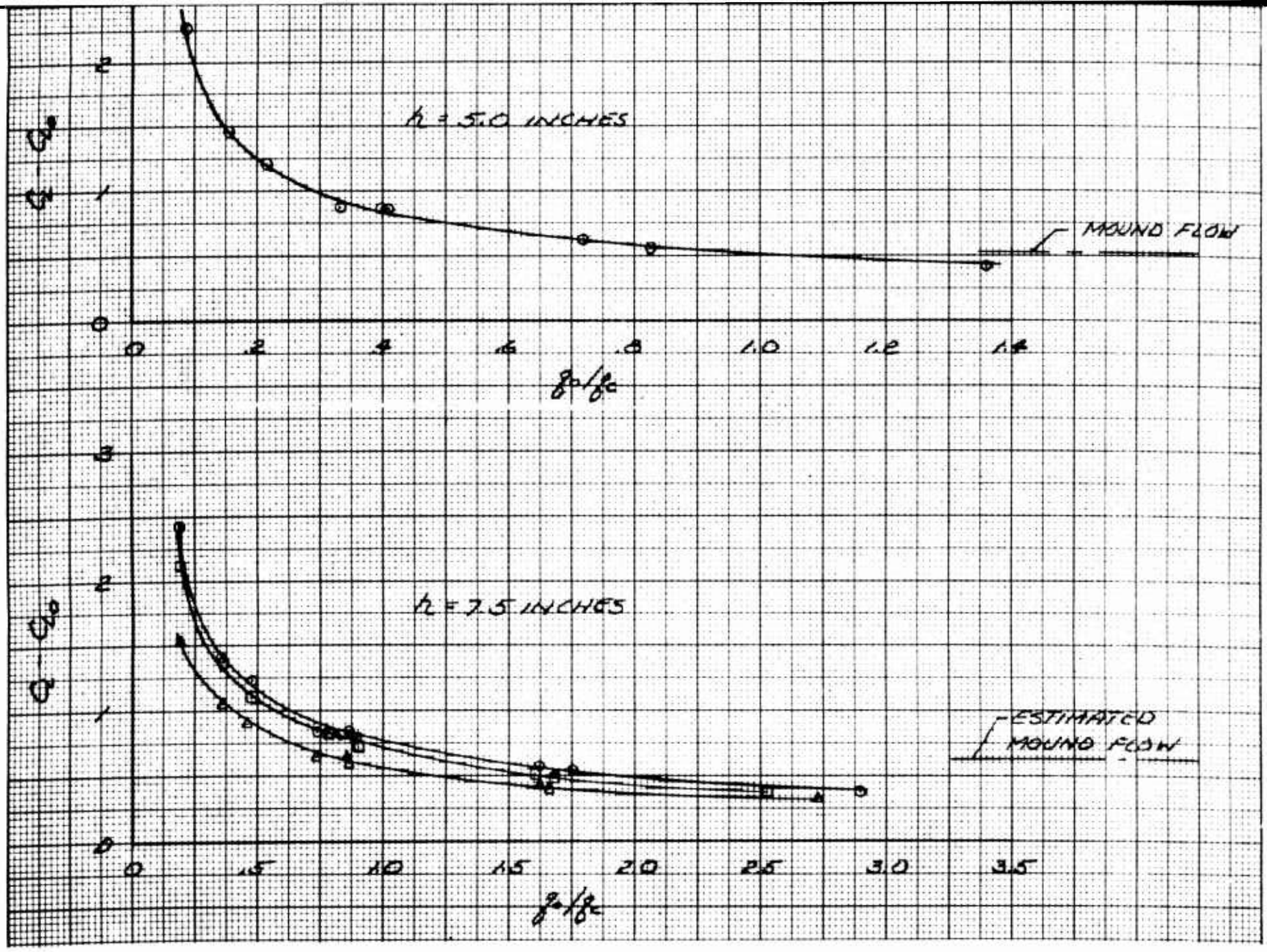

Fig. 3 Variation of $C_L - C_{Lo}$ with q_o/q_c

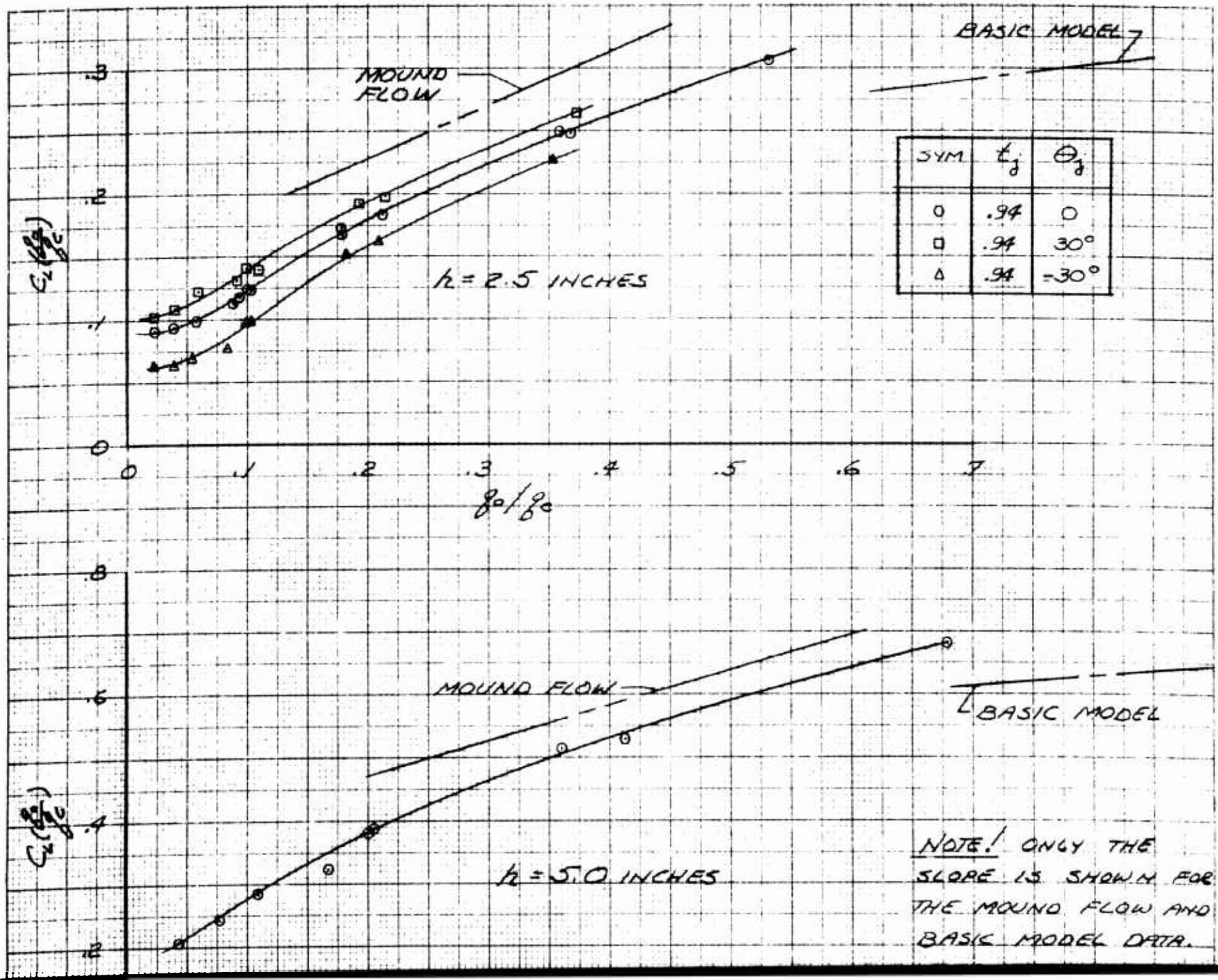
BASIC MODEL
MOUND FLOW
SYM
ξ_j
Θ_j
0
.94
0
□
.94
30°
△
.94
-30°
h = 2.5 INCHES
$C_L(\frac{q_o}{q_c})$
.3
.2
.1
0
0
.1
.2
.3
.4
.5
.6
.7
q_o/q_c
.8
.6
.4
.2
MOUND FLOW
BASIC MODEL
h = 5.0 INCHES
NOTE! ONLY THE SLOPE IS SHOWN FOR THE MOUND FLOW AND BASIC MODEL DATA.

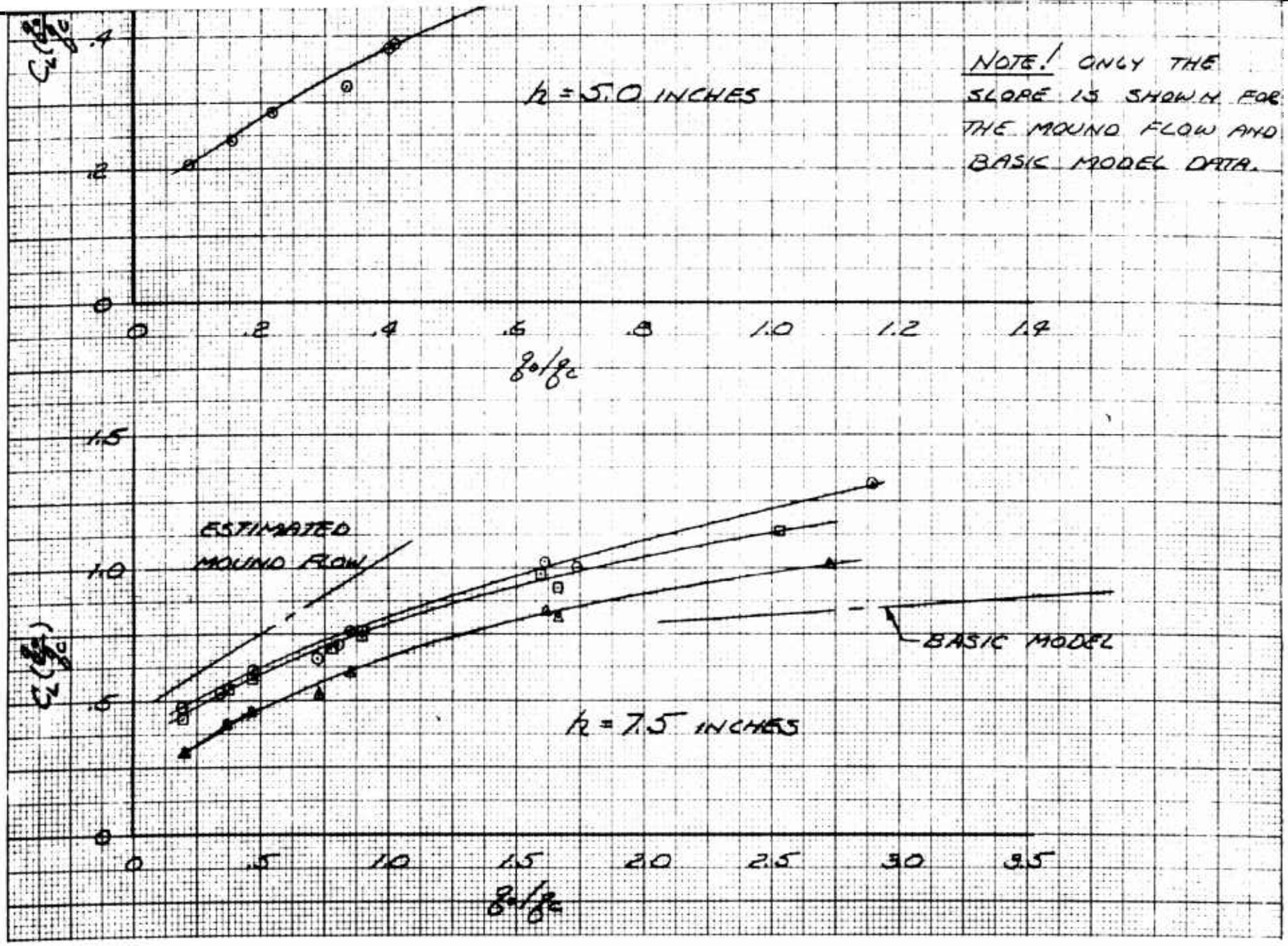

Fig. 4 Variation of $C_L q_o/q_c$ with q_o/q_c

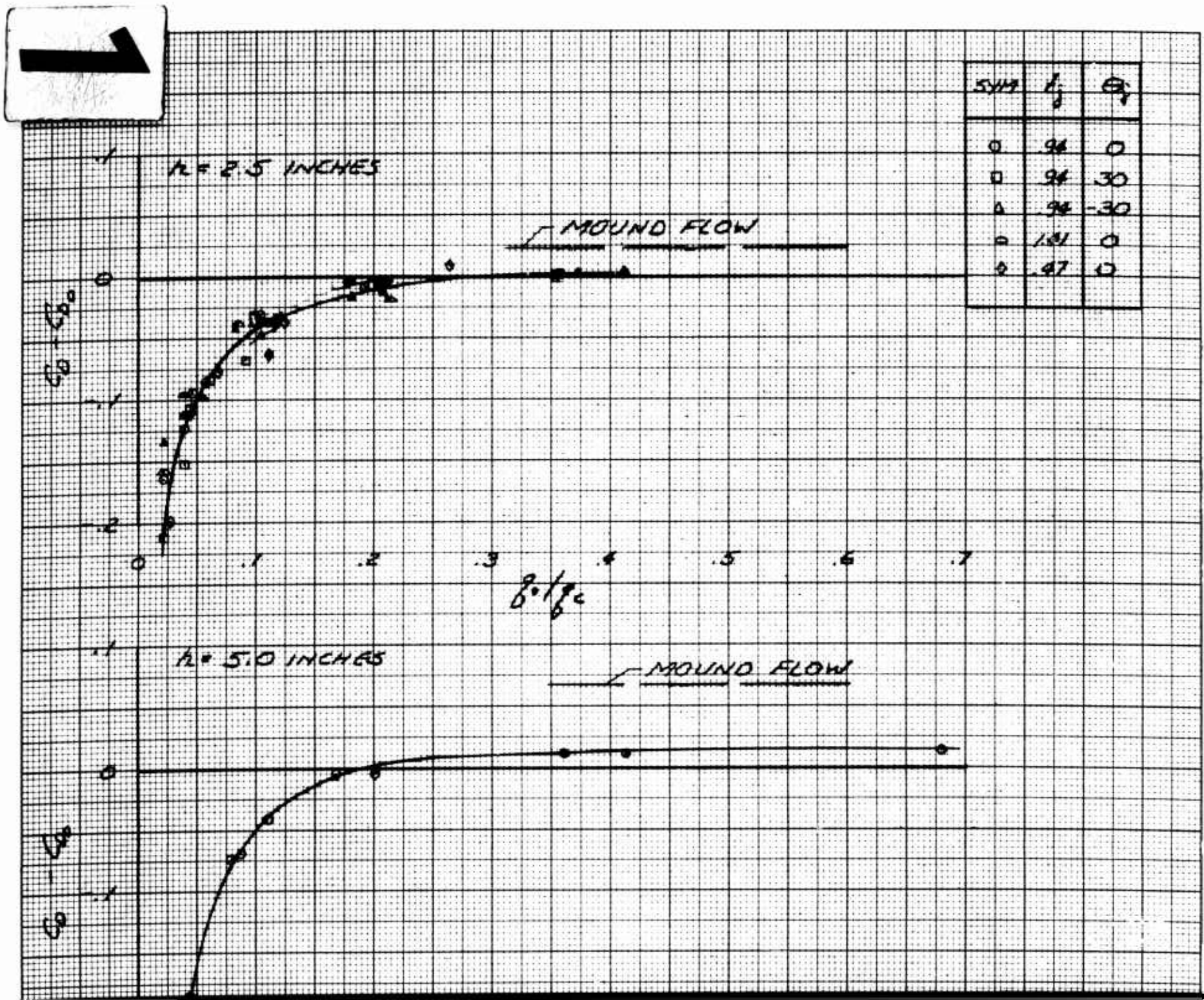
7
h = 2.5 INCHES
MOUND FLOW
sym
h_j
θ_j
94
0
94
30
94
-30
151
0
47
0
C_{D_0}
C_D
$\theta \cdot 1/\theta_c$
h = 5.0 INCHES
MOUND FLOW

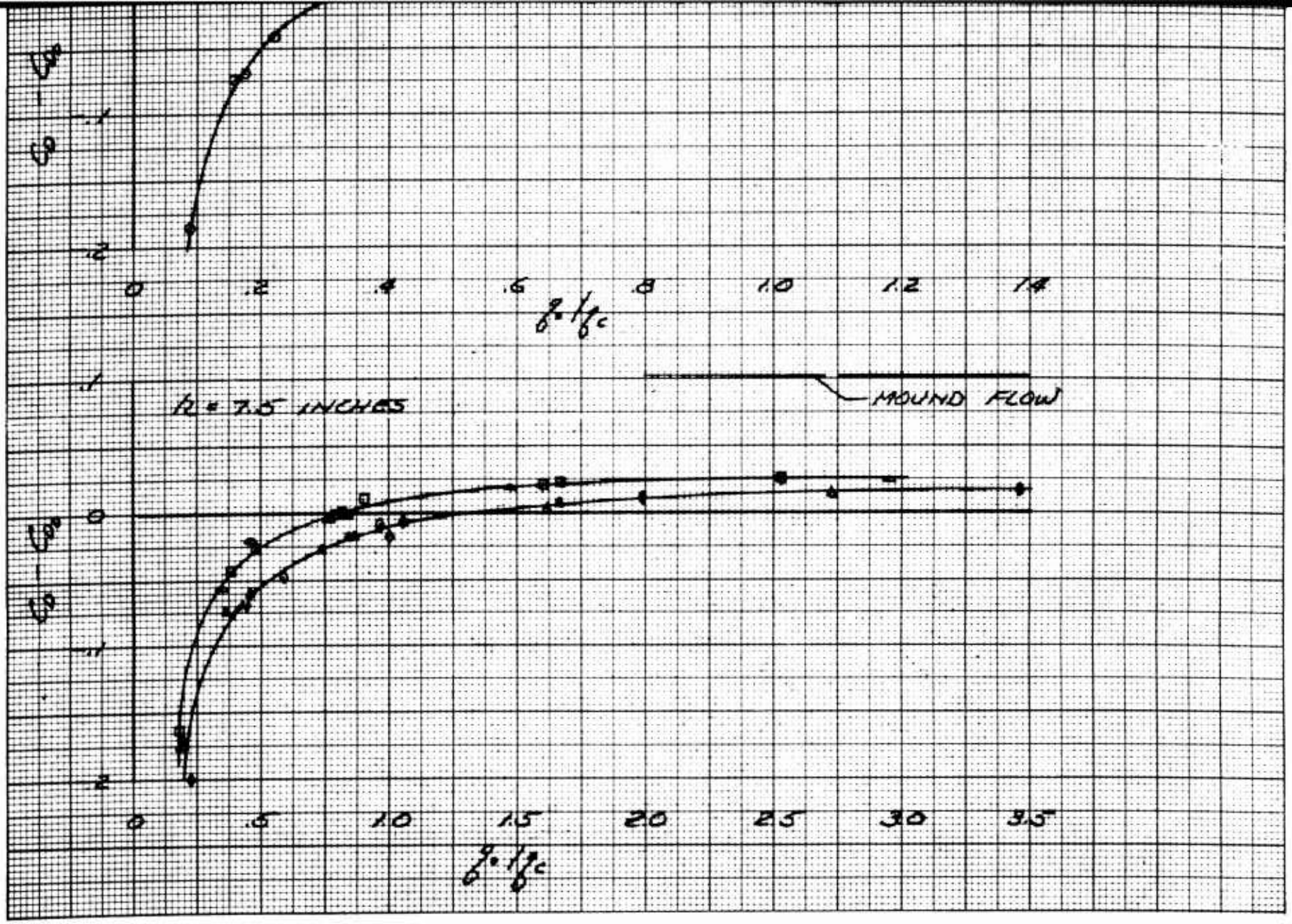

Fig. 5 Variation of $C_D - C_{Do}$ with q_o/q_c

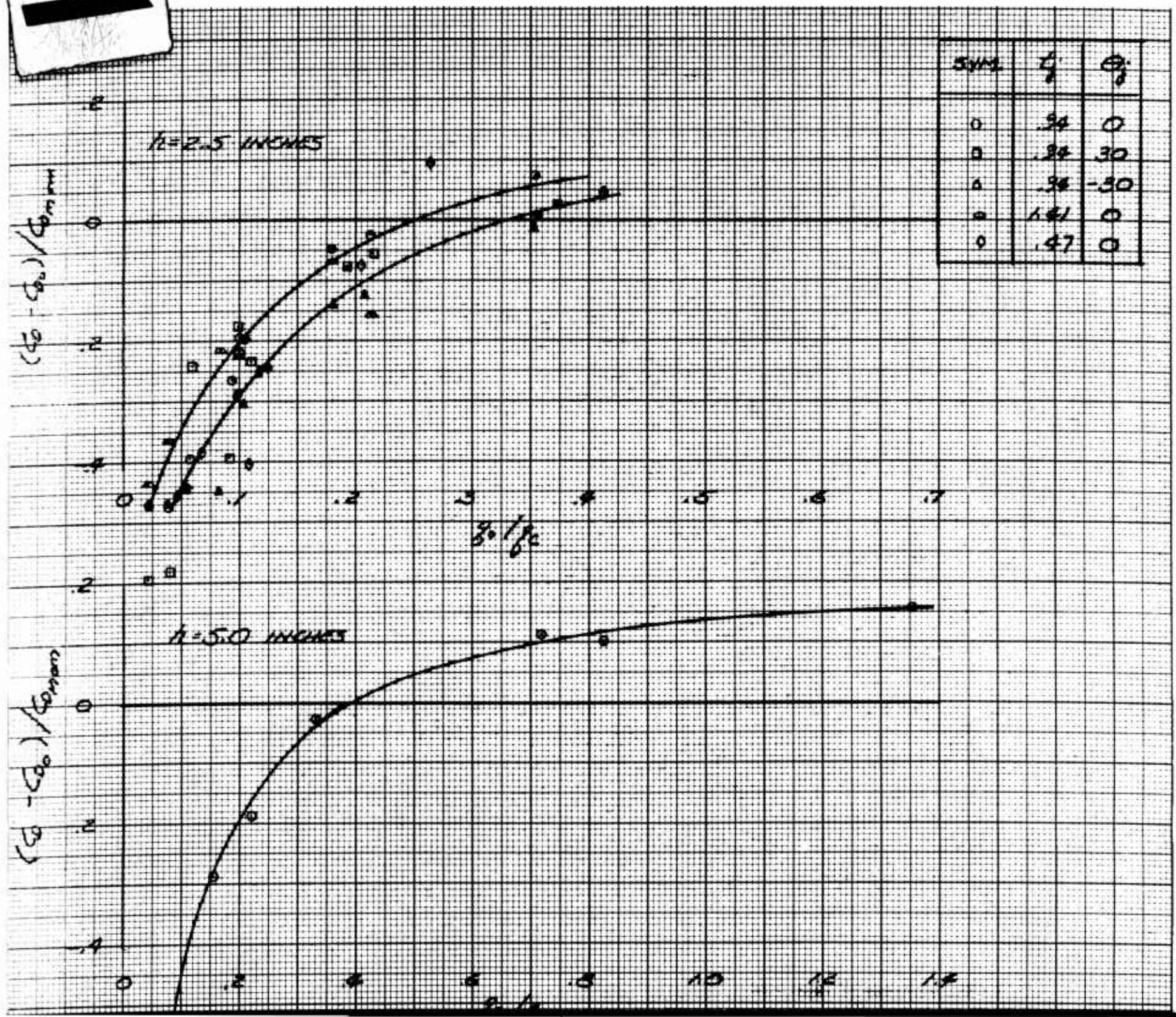
SYM.
C_ϕ'
ϕ_ϕ'
○ .94 0
□ .84 30
△ .96 -30
▽ 1.41 0
◇ .47 0
h=2.5 INCHES
$(\sigma_\phi - \sigma_\phi')/\sigma_{\phi max}$
σ_ϕ'/σ_c
h=5.0 INCHES
$(\sigma_\phi - \sigma_\phi')/\sigma_{\phi max}$
σ_ϕ'/σ_c

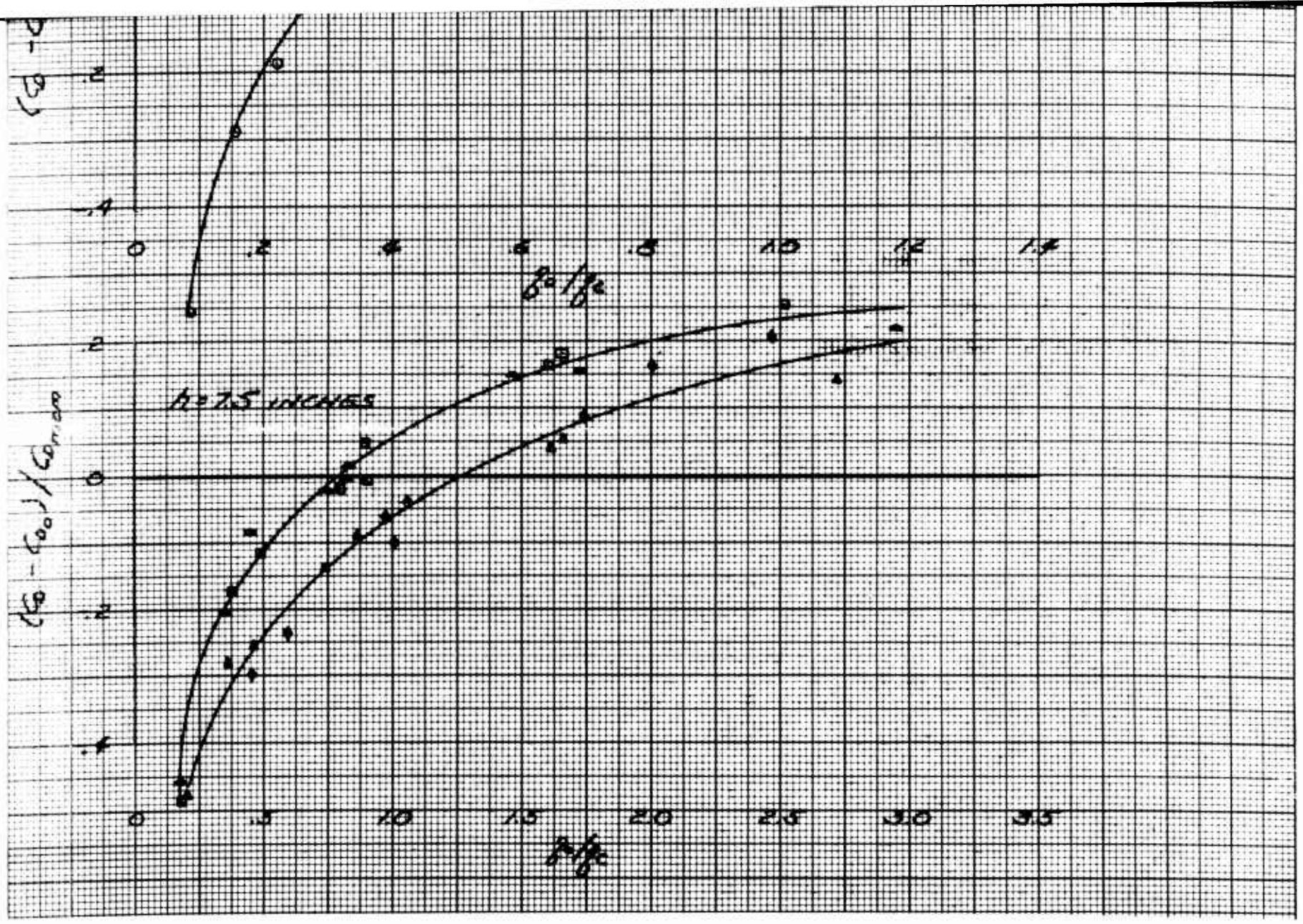

Fig. 6 Variation of $(C_D - C_{Do})/C_{Dmom}$ with q_o/q_c

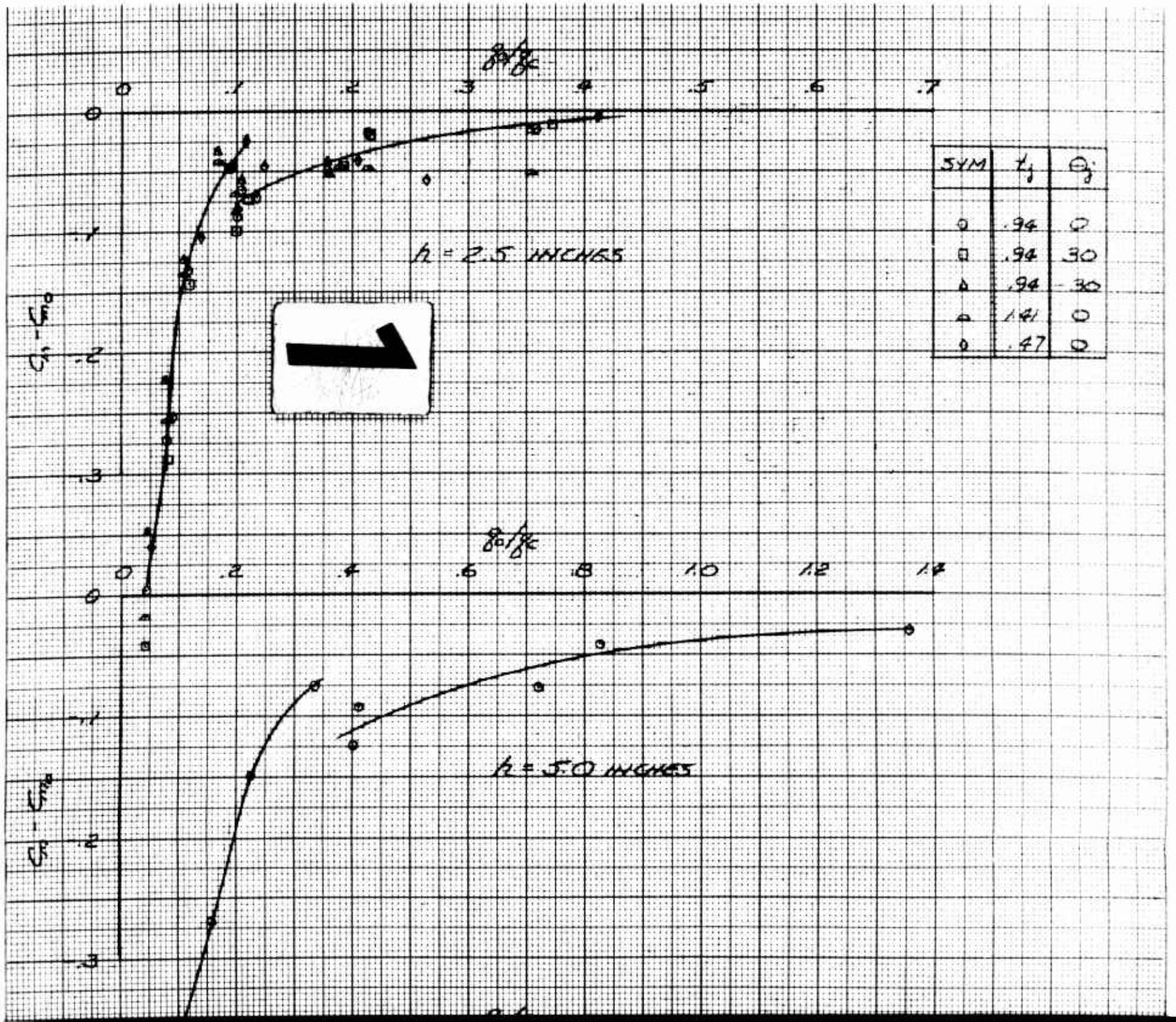
h = 2.5 INCHES
h = 5.0 INCHES
SYM
Y_j
Θ_j
.94
0
.94
30
.94
-30
.141
0
.47
0

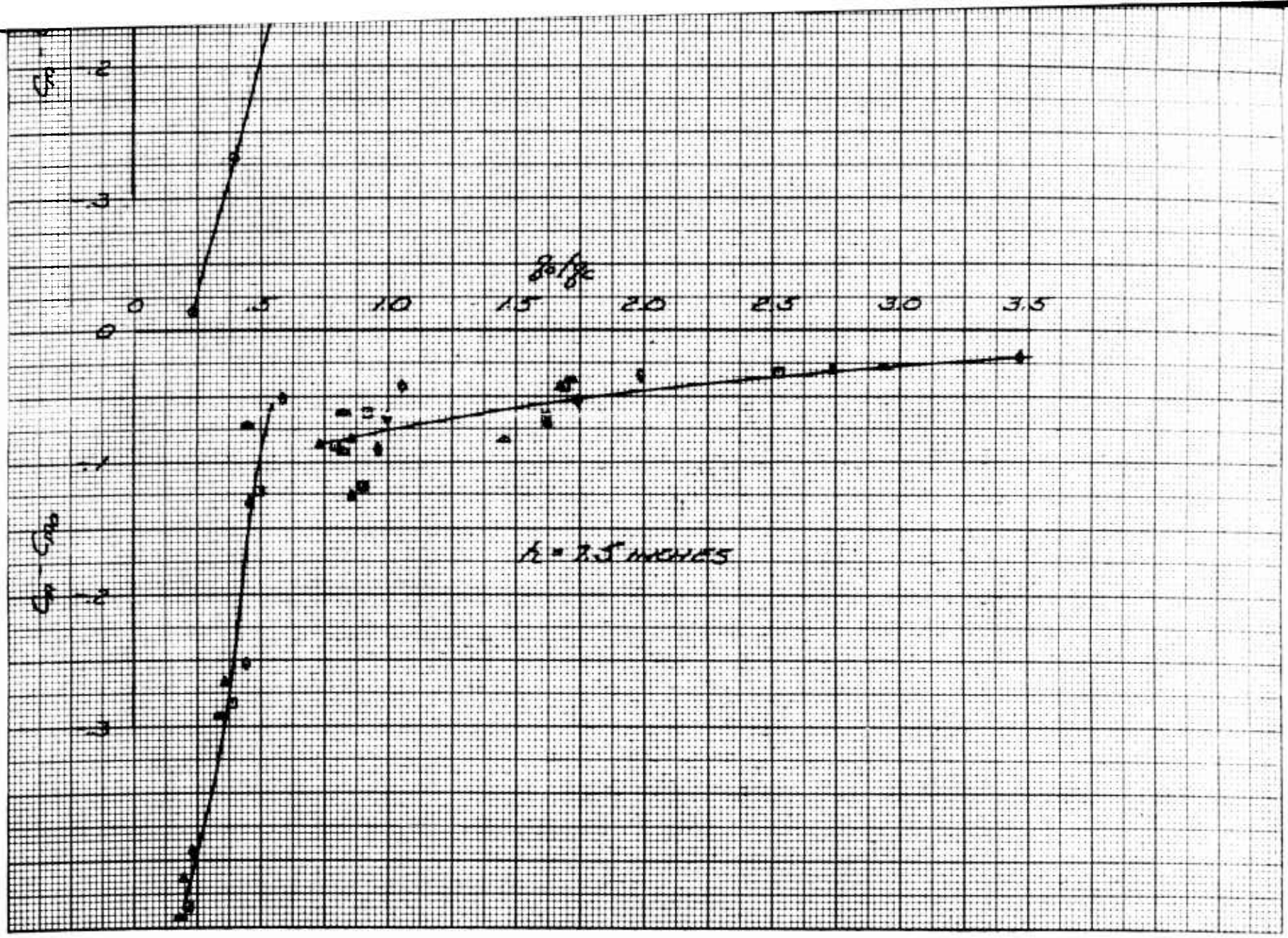

Fig. 7 Variation of $(C_m - C_{mo})$ with q_o/q_c

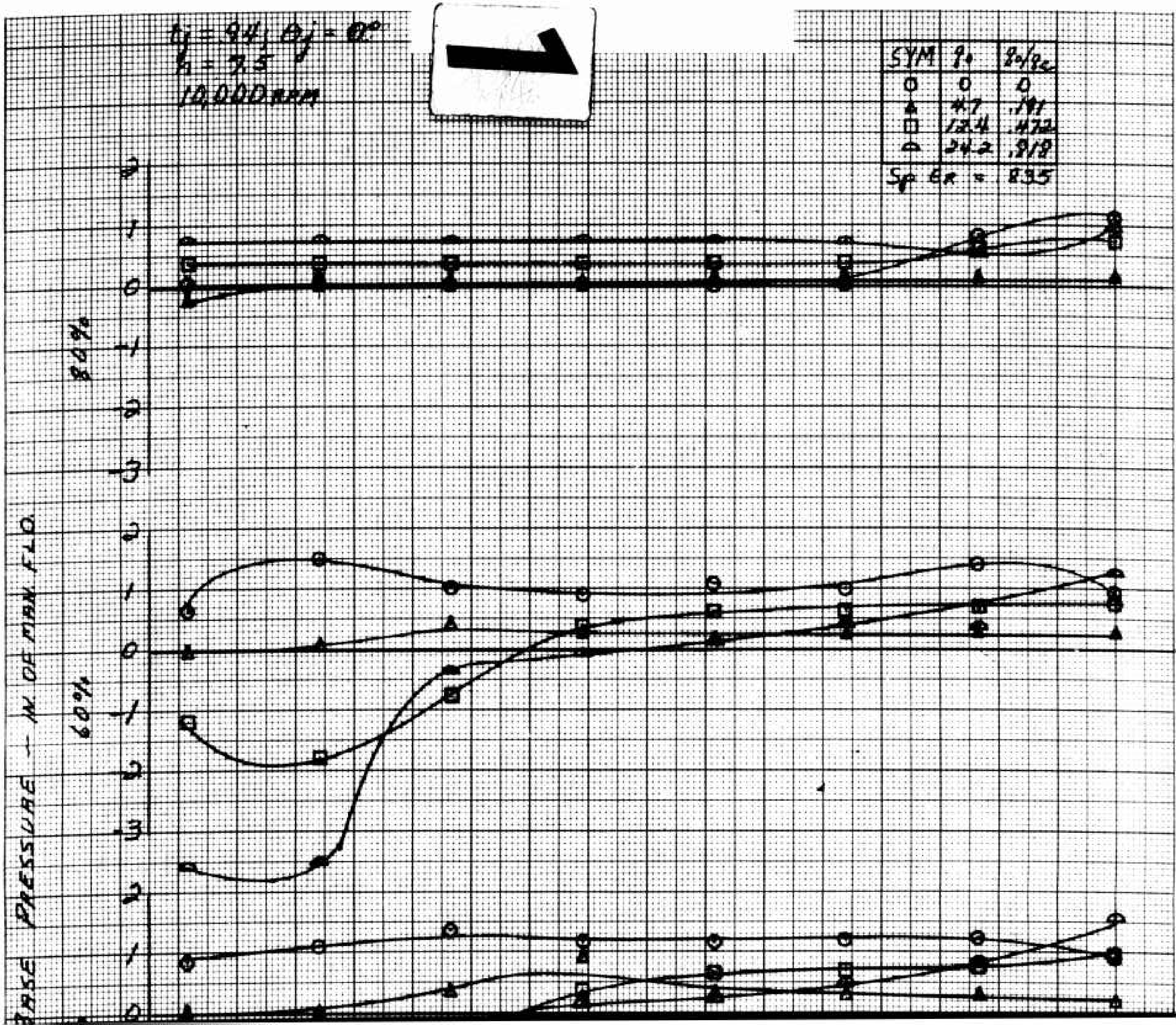

tj = 94; θj = 0°
h = 7.5
10,000 RPM
SYM | q_0 | q_0/q_c
○ | 0 | 0
▲ | 4.7 | .191
□ | 12.4 | .472
◓ | 24.2 | .918
S_p G_R = .835
80%
60%
BASE PRESSURE — IN. OF MAN. FLD.
2
1
0
-1
-2
-3

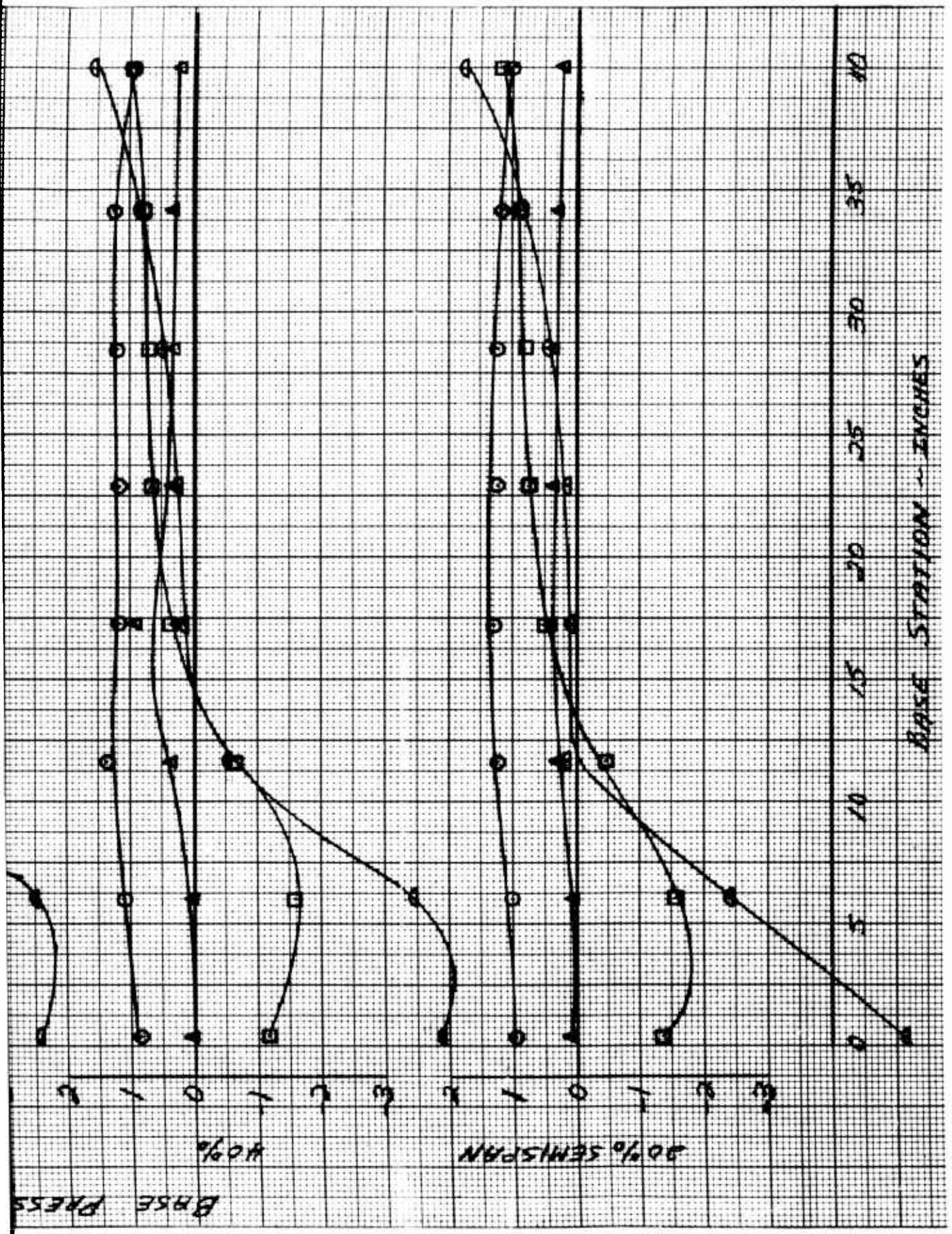

Fig. 8 Base Pressure Data, $h = 7.5$, $t_j = .94$, $\theta_j = 0$, 10000 rpm

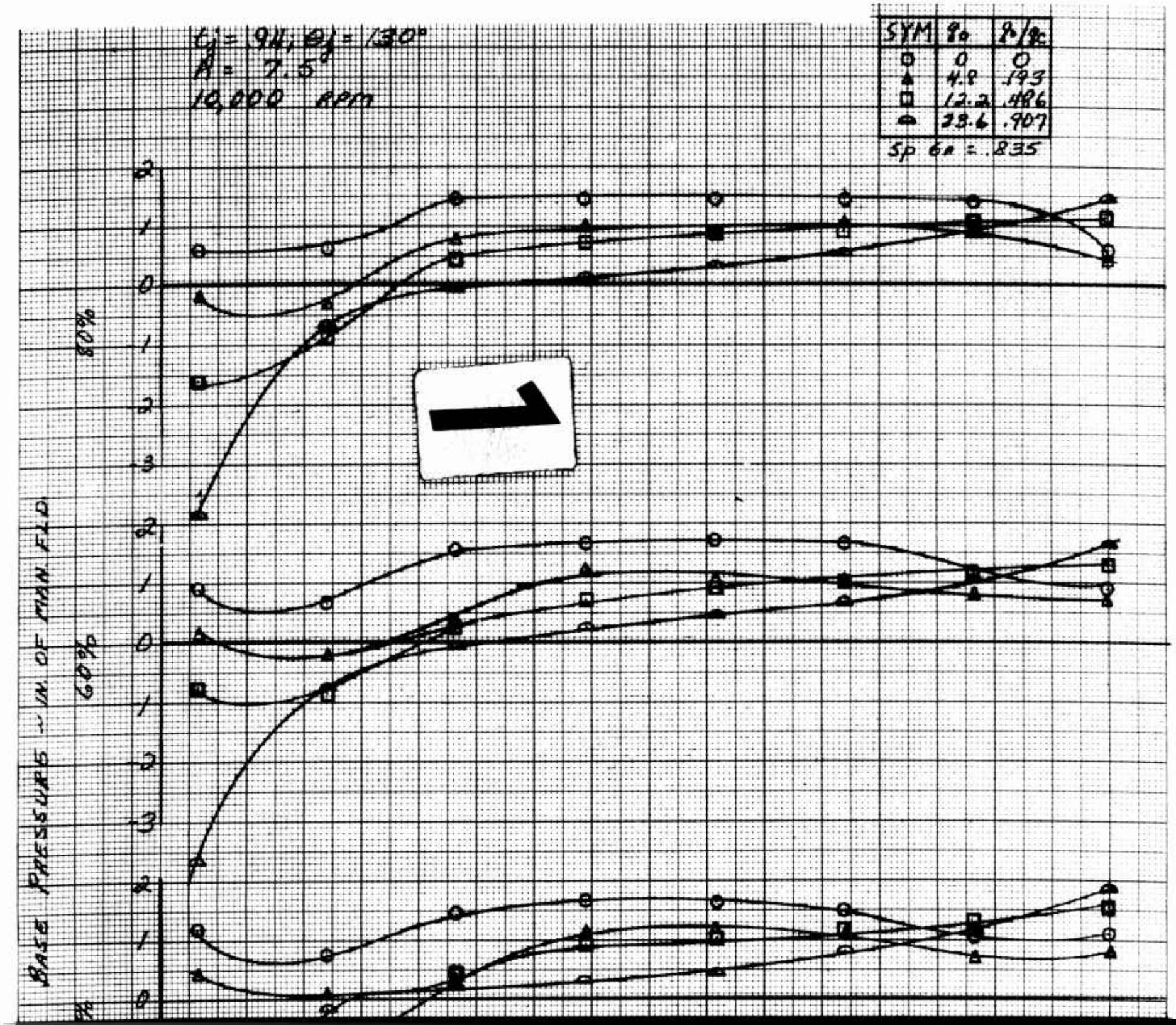
C_j = .94, Θ_j = 130°
β = 7.5°
10,000 RPM
SYM | β_0 | β/β_c
□ | 0 | 0
▲ | 4.8 | .193
■ | 12.2 | .486
◆ | 23.4 | .907
Sp 6ℓ = .835
80%
60%
BASE PRESSURE - IN OF MAN FLD

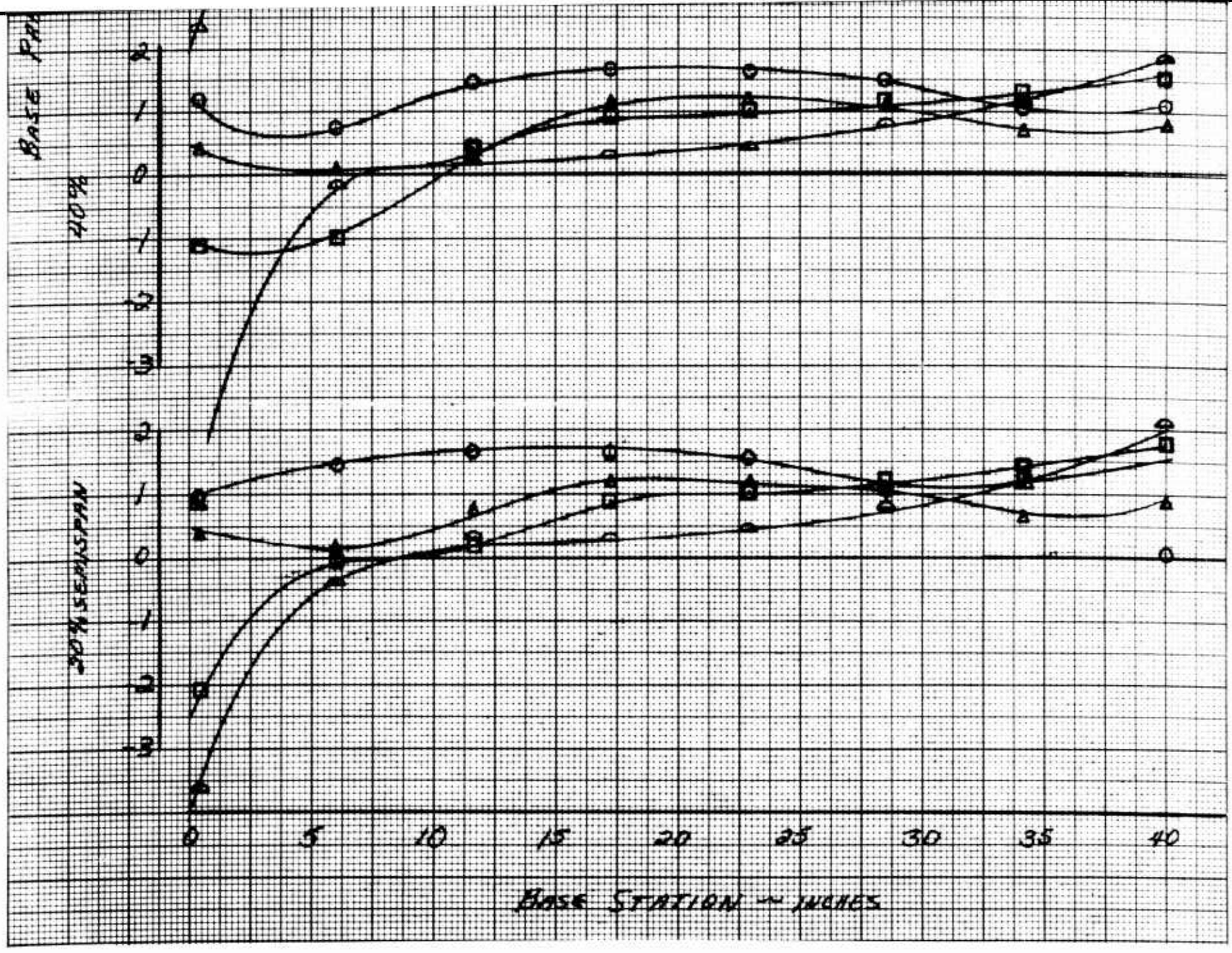

Fig. 9 Base Pressure Data, h = 7.5, t_j = .94, θ_j = 30, 10000 rpm

SYM
Sp.Gr. = .835
60%
80%
PHASE PRESSURE — IN OF MAN FLD
1

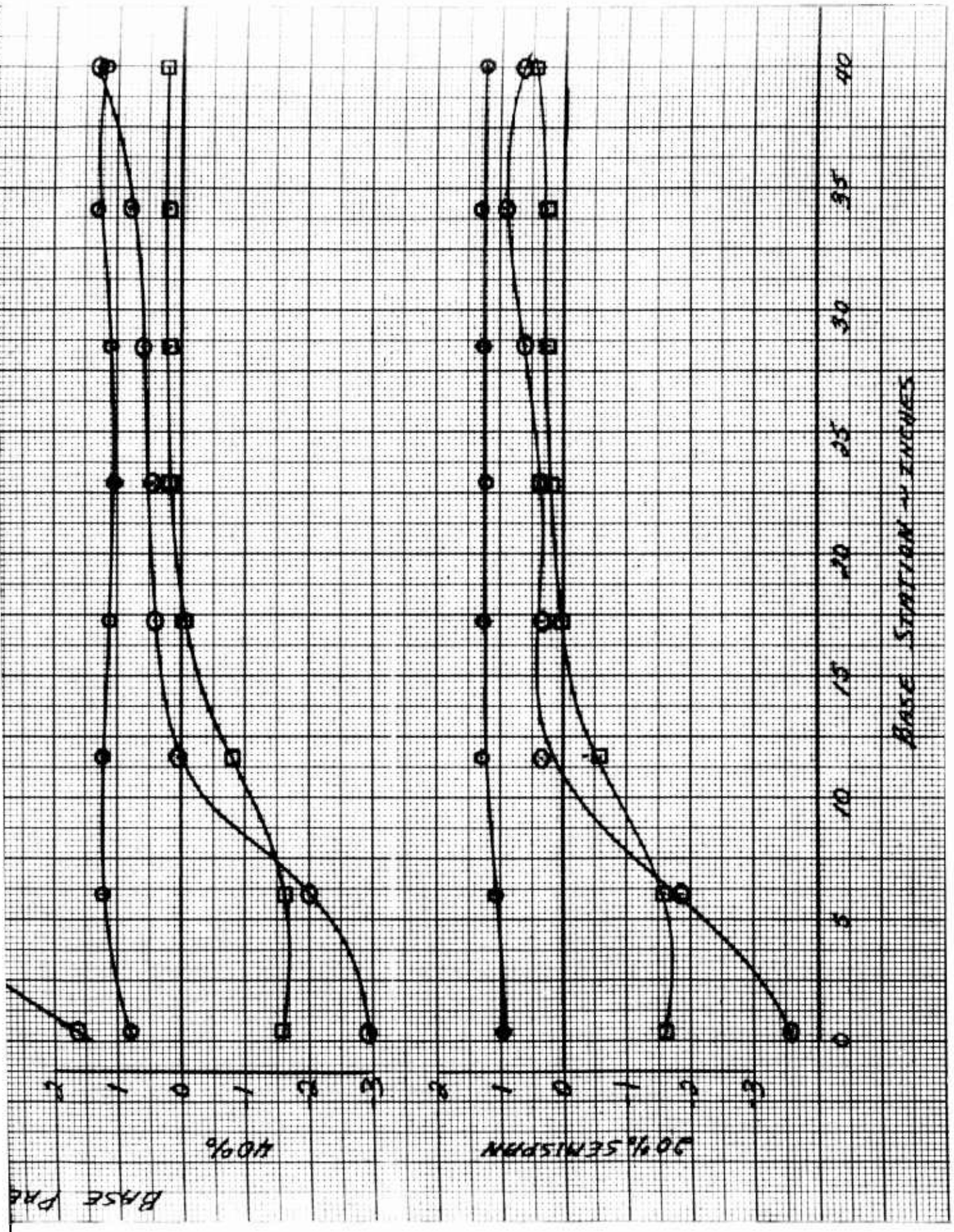

Fig. 10 Base Pressure Data, h = 7.5, t_j = .94, θ_j = -30, 10000 rpm

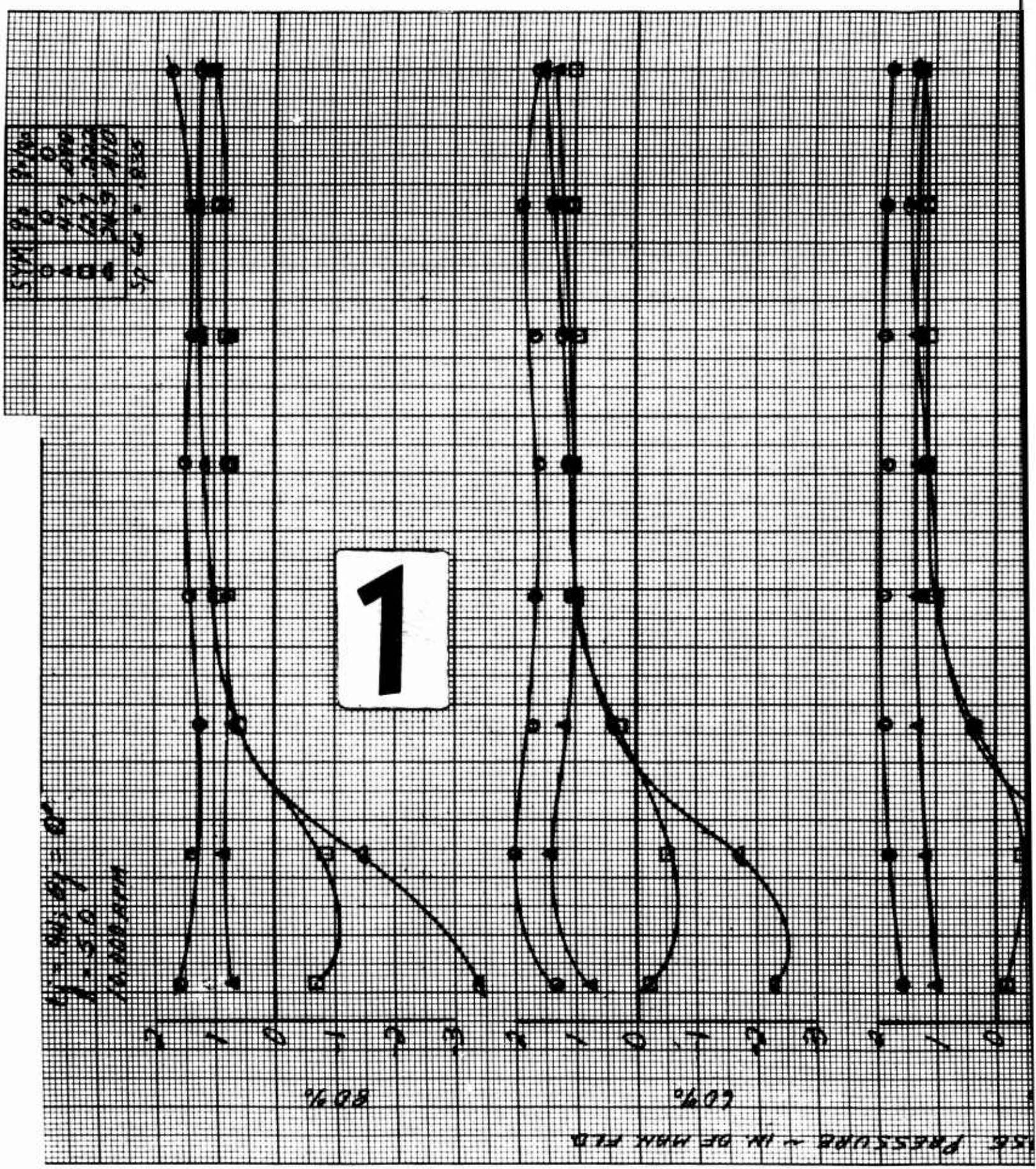
1
80%
60%

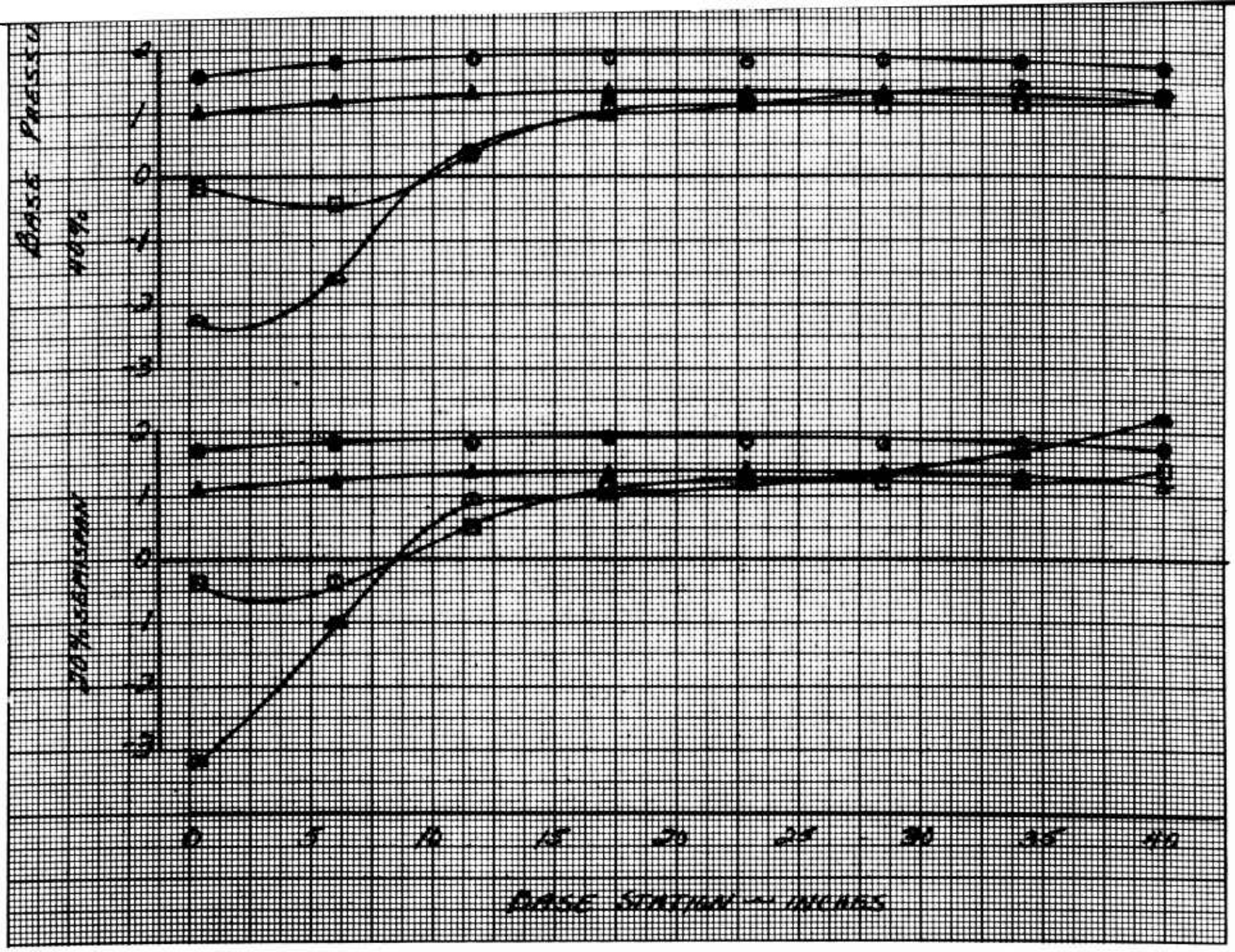

Fig. 11 Base Pressure Data, h = 5.0, t_j = .94, v_j = 0, 10000 rpm

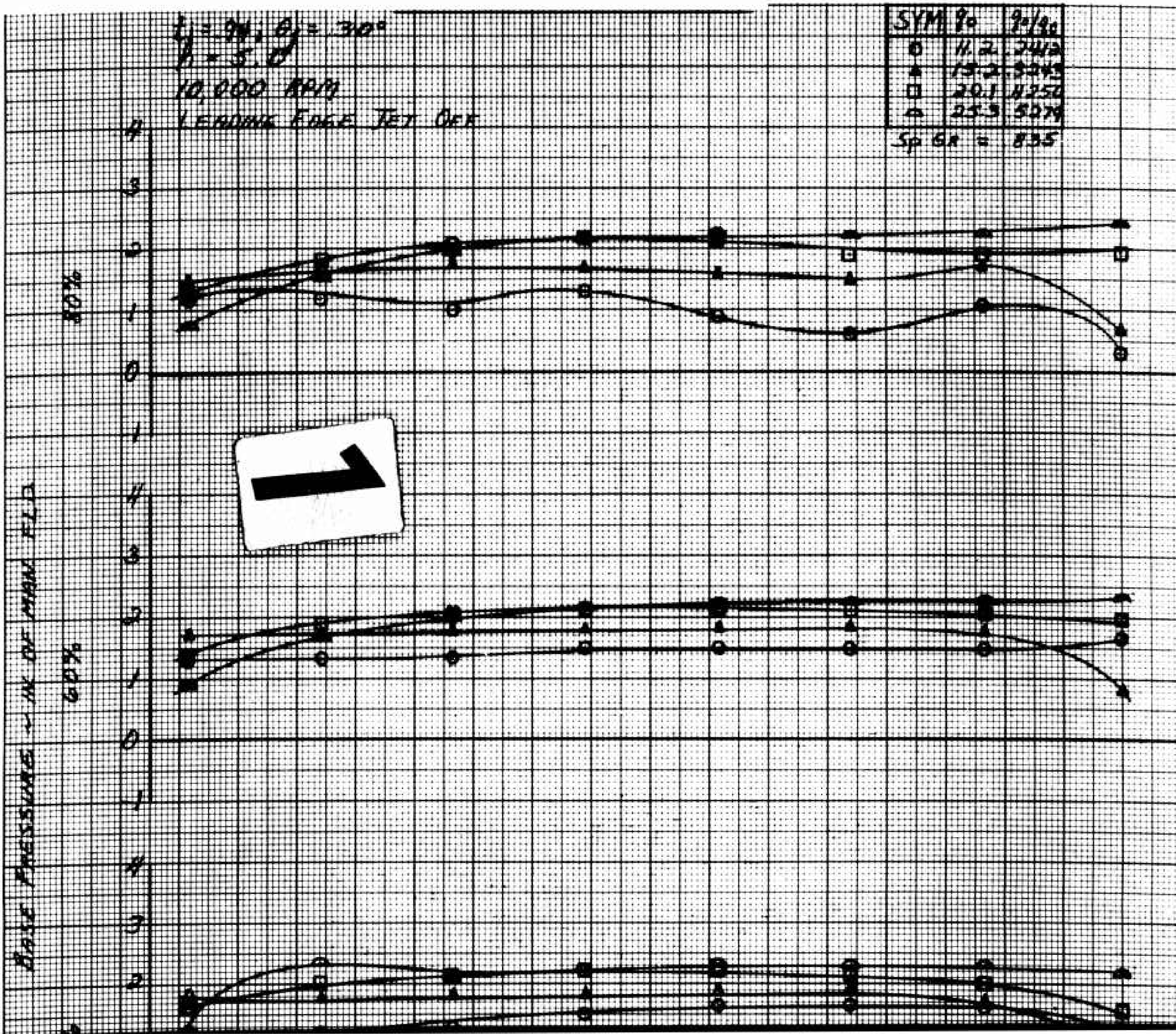

t/j = .94; θj = 30°
h = 5.0
10,000 RPM
LEADING EDGE JET OFF
SYM | P0 | P0/PD
11.2 | .2412
15.2 | .3245
20.1 | .4250
25.3 | .5279
Sp Gr = .835
80%
60%
BASE PRESSURE ~ IN OF MAN FLD
4
3
2
1
0
1

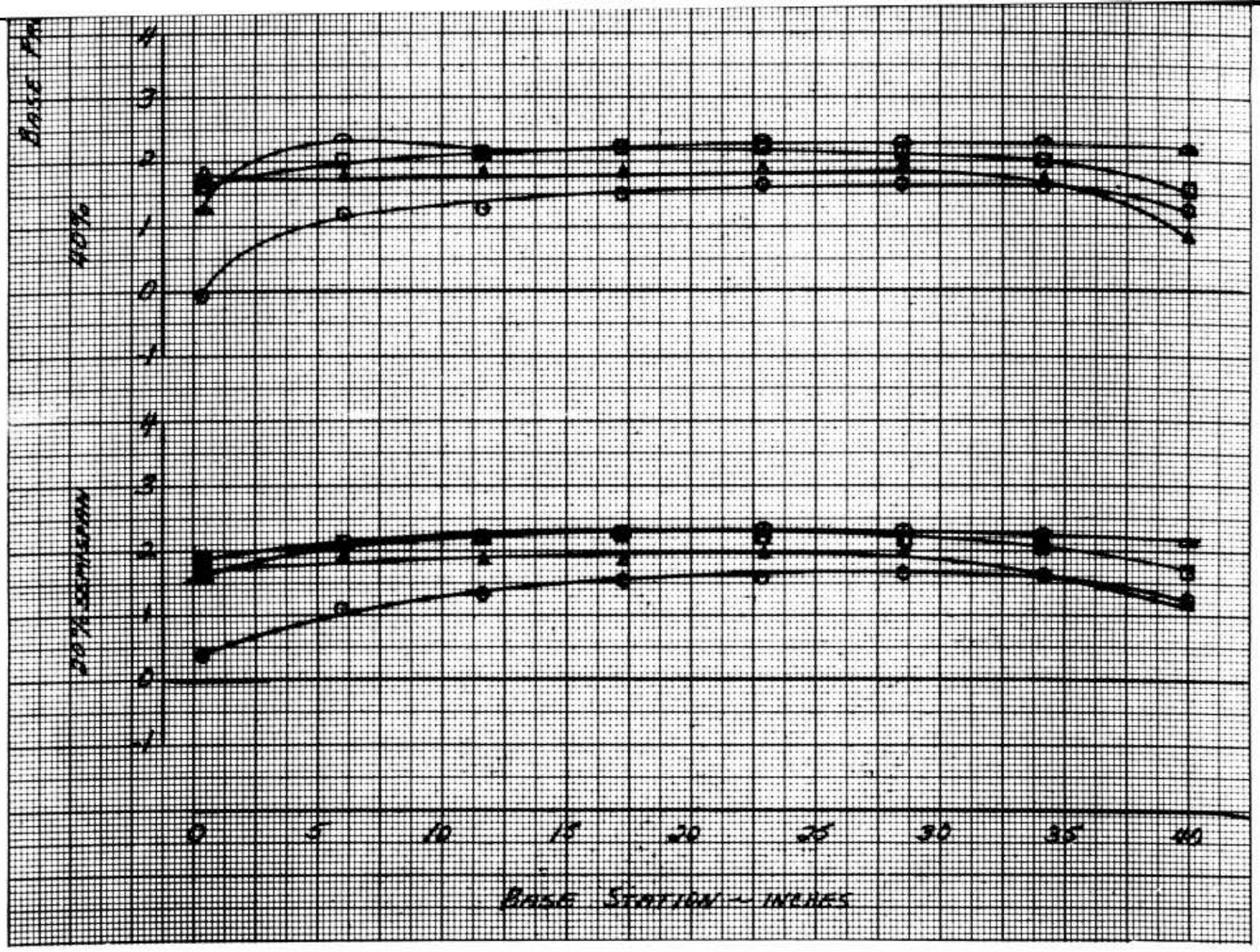

Fig. 12 Base Pressure Data, h = 5.0, t_j = .94, v_j = 30, 10000 rpm, Leading Edge Jet Off

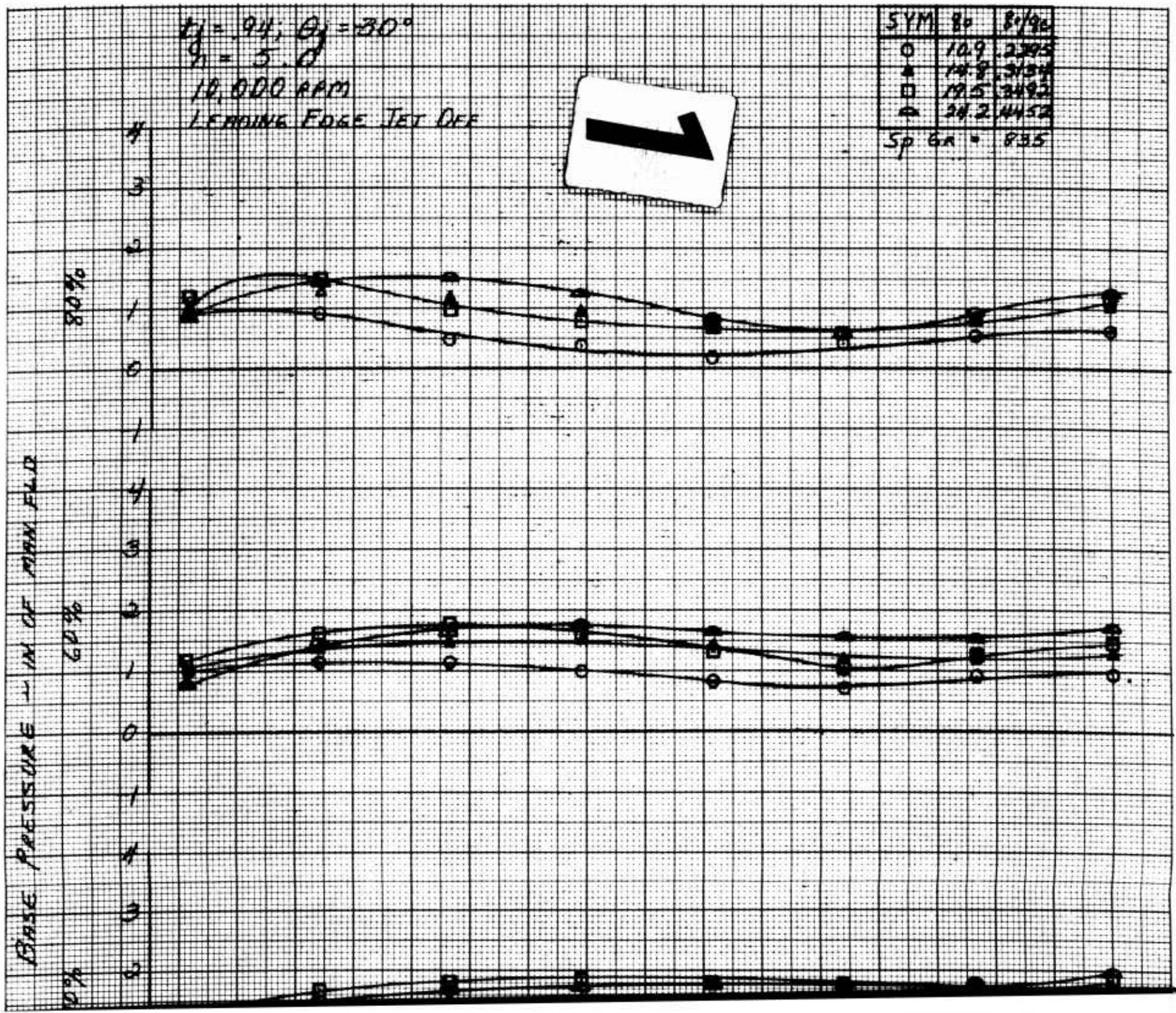
t_j = .94; θ_j = 30°
h = 5.0
10,000 RPM
LEADING EDGE JET OFF
SYM | β_0 | β/β_0
○ | 10.9 | .2395
▲ | 14.8 | .3134
□ | 15.5 | .3482
◇ | 20.2 | .4452
S_p G_R = .835
80%
60%
0%
BASE PRESSURE - IN OF MAN ELD

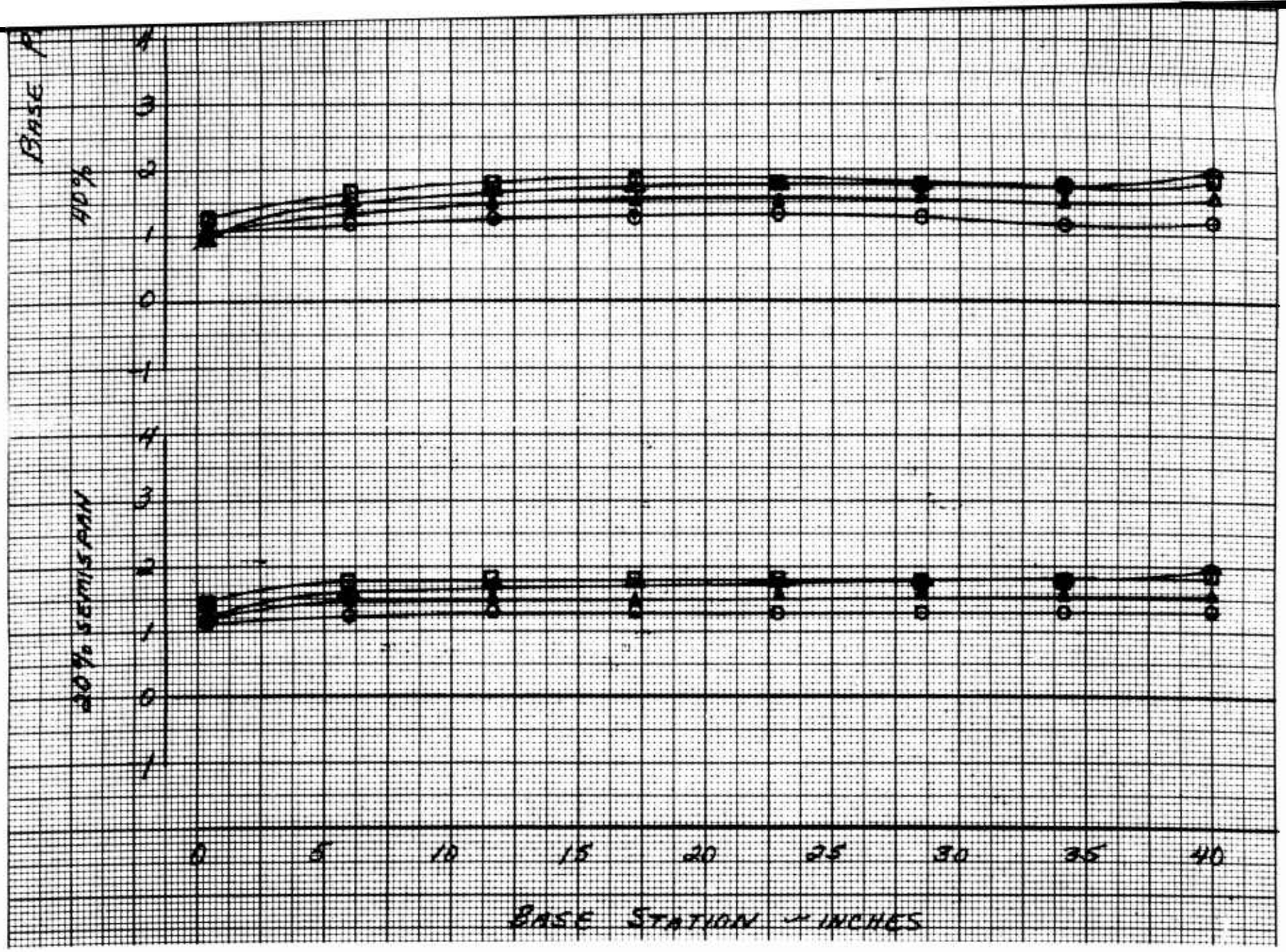

Fig. 13 Base Pressure Data, h = 5.0, t_j = .94, α_j = -30, 10000 rpm, Leading Edge Jet Off

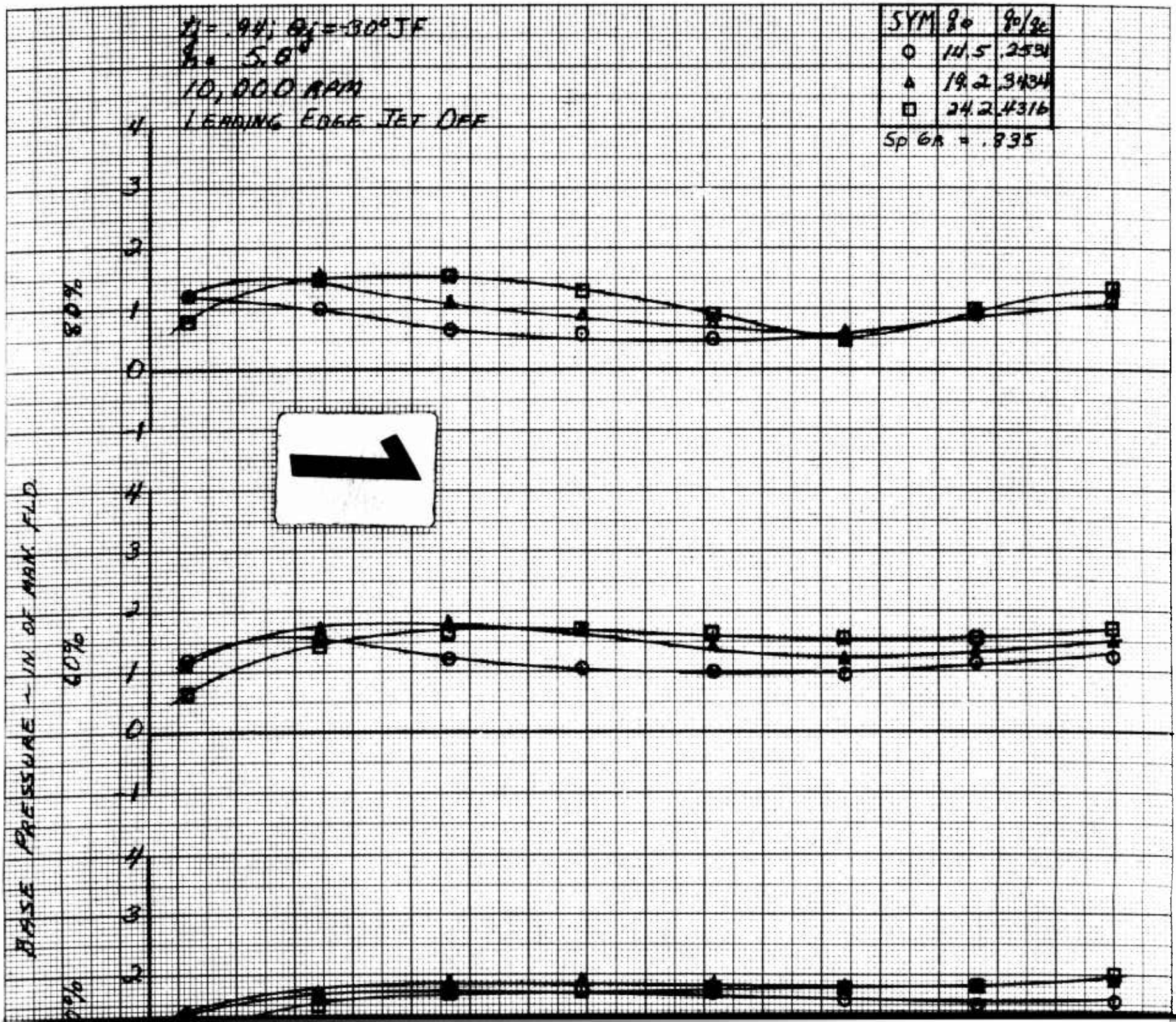
η_j = .94; θ_j = 30° JF
α_b = 5.8°
10,000 RPM
LEADING EDGE JET OFF
SYM | q_ϕ | q_ϕ/q_c
○ | 14.5 | .2534
△ | 19.2 | .3434
□ | 24.2 | .4316
Sp Gr = .835
80%
60%
BASE PRESSURE - IN. OF MAK. FLD
4
3
2
1
0
-1
-2
-3
-4

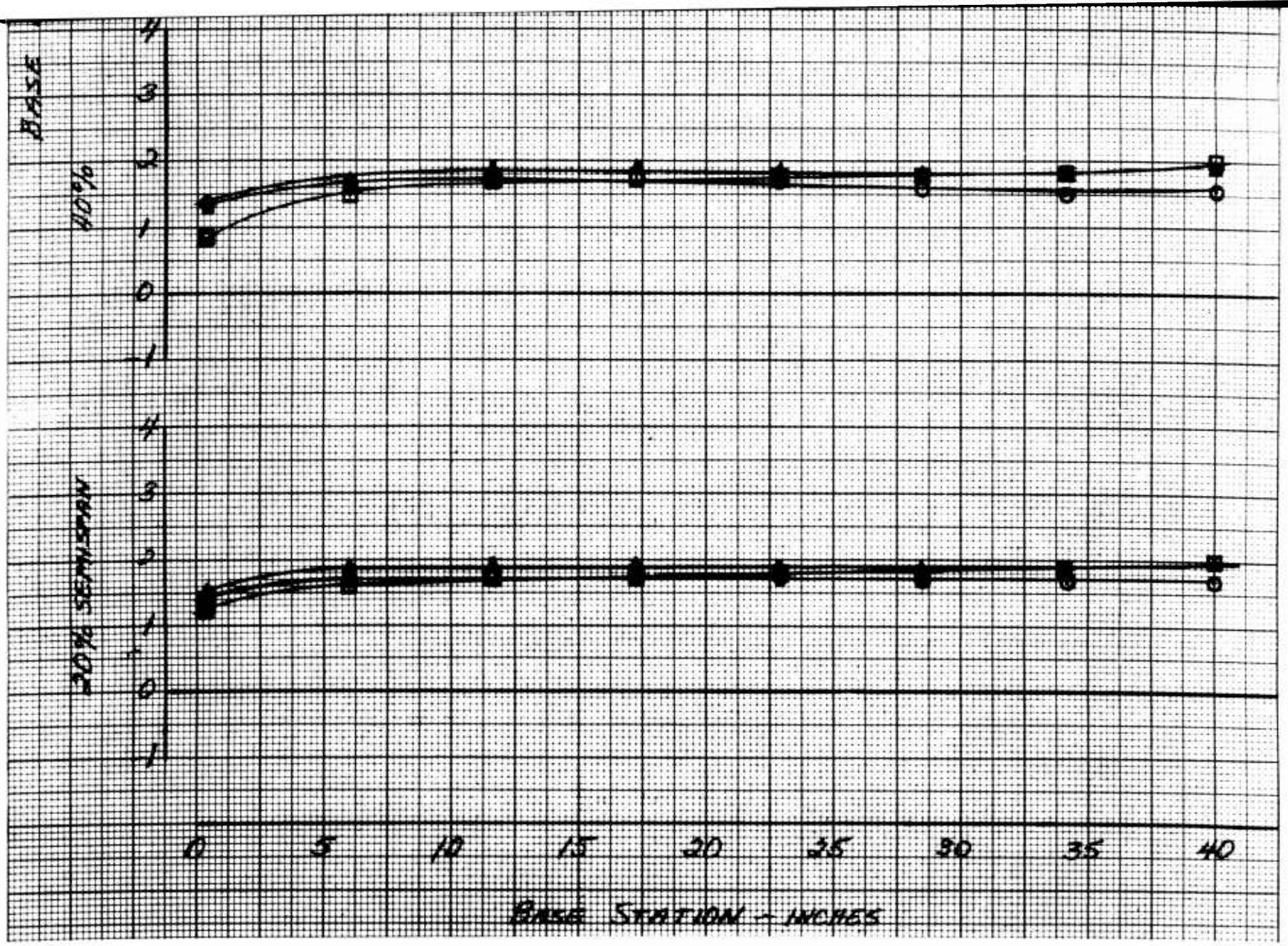

Fig. 14 Base Pressure Data, h = 5.0, t_j = .94, γ_j = -30JF, 10000 rpm, Leading Edge Jet Off

1

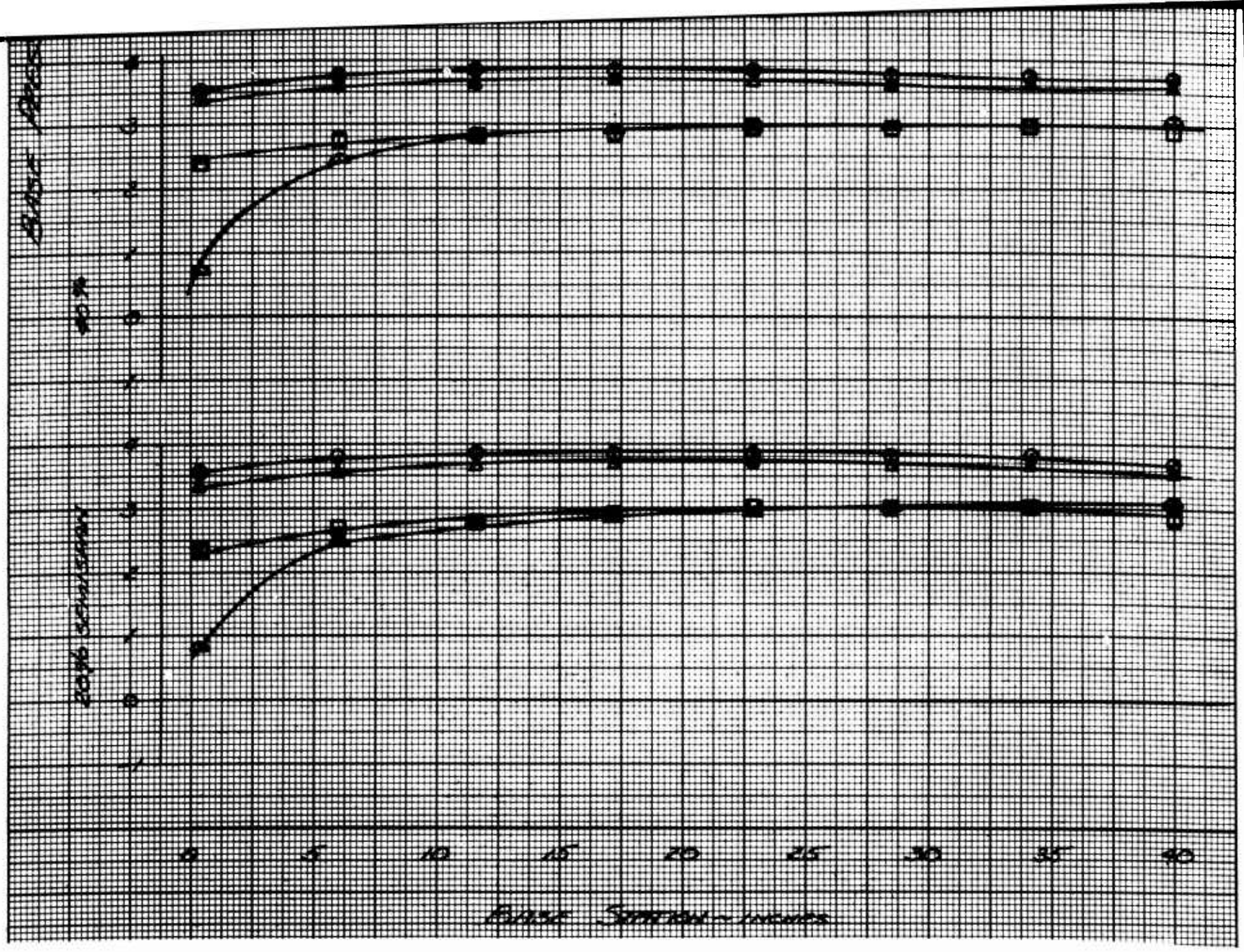

Fig. 15 Base Pressure Data, h = 2.5, t_j = .94, θ_j = 0, 10000 rpm

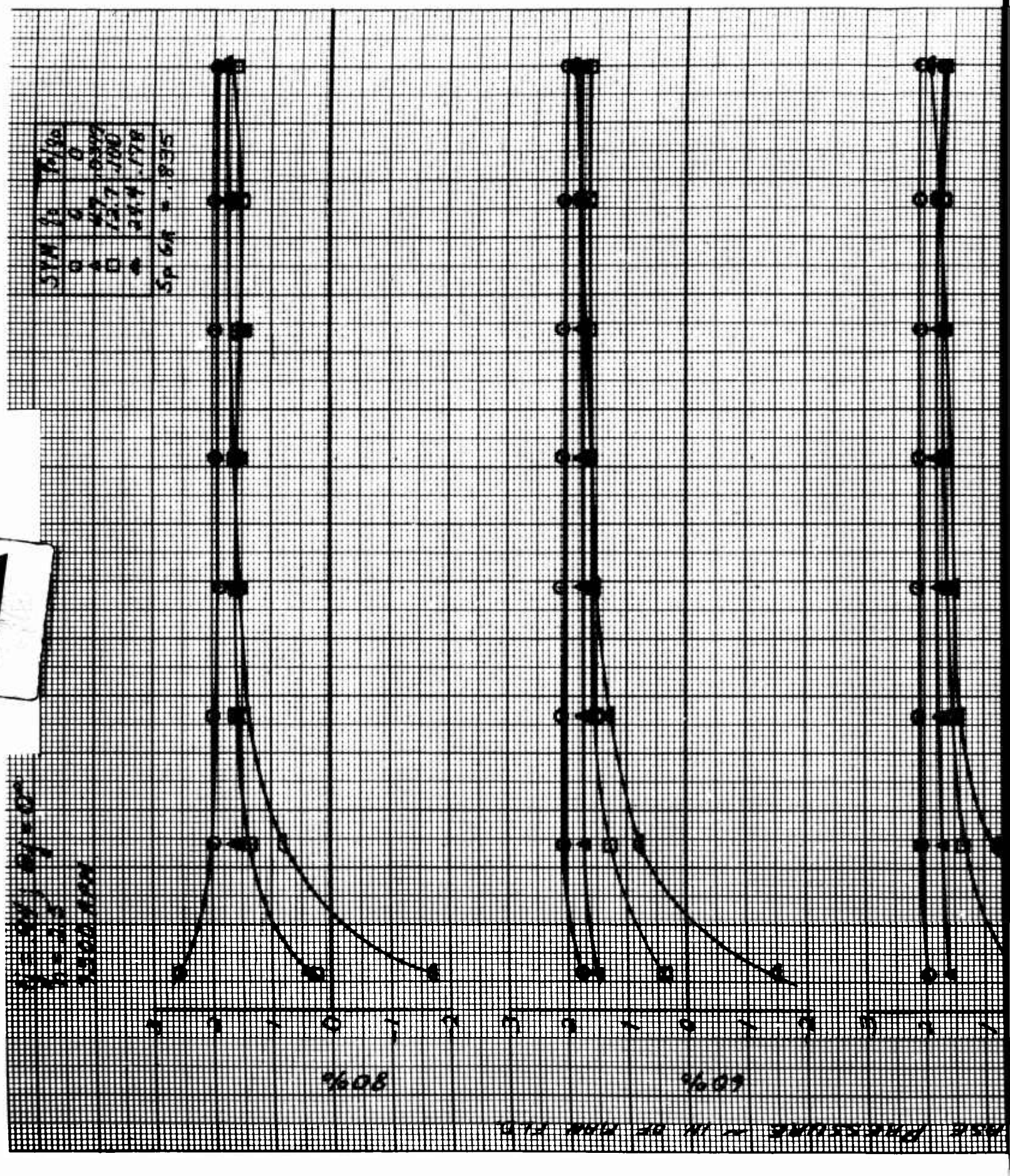
1

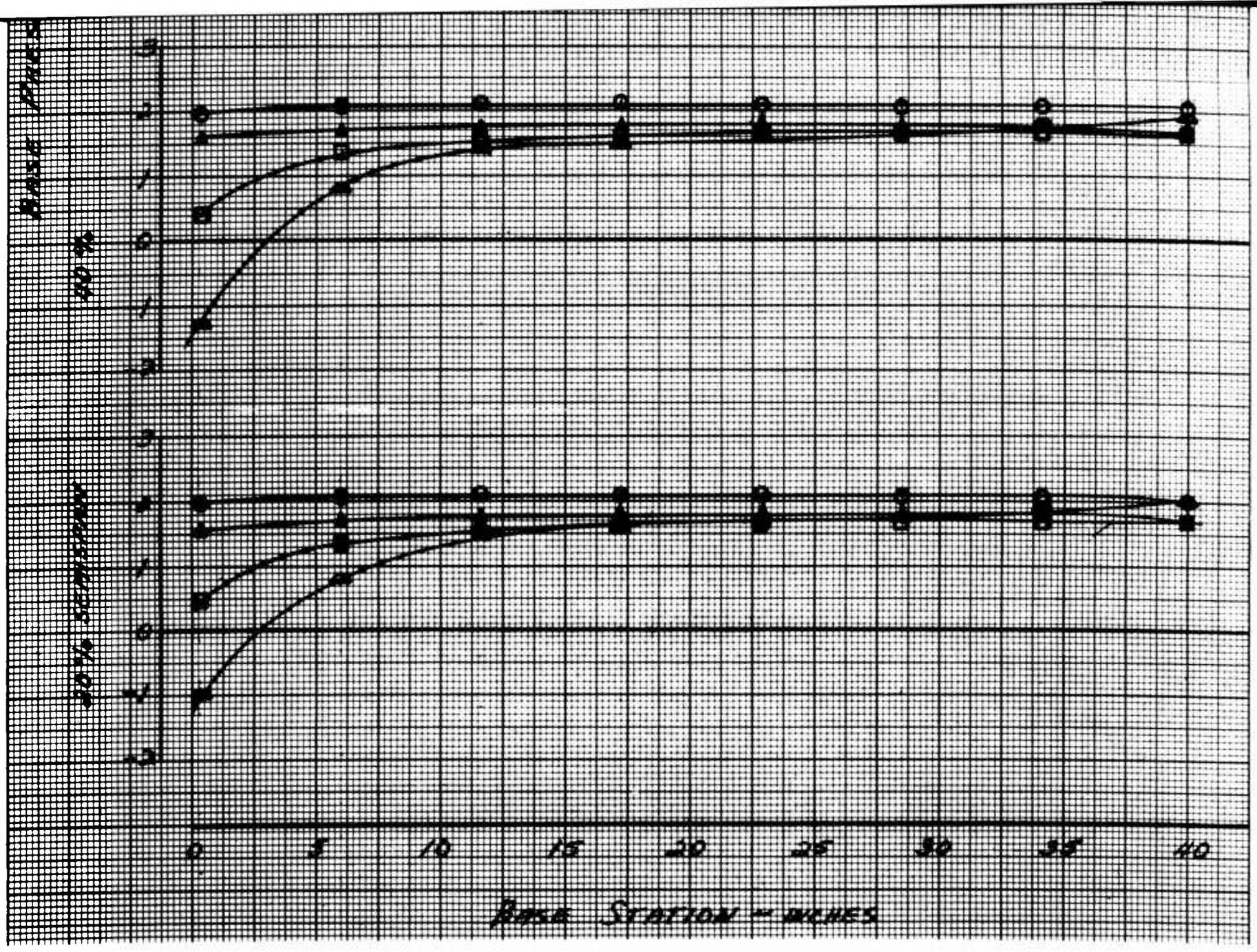

Fig. 16 Base Pressure Data, h = 2.5, t_j = .94, θ_j = 0, 7300 rpm

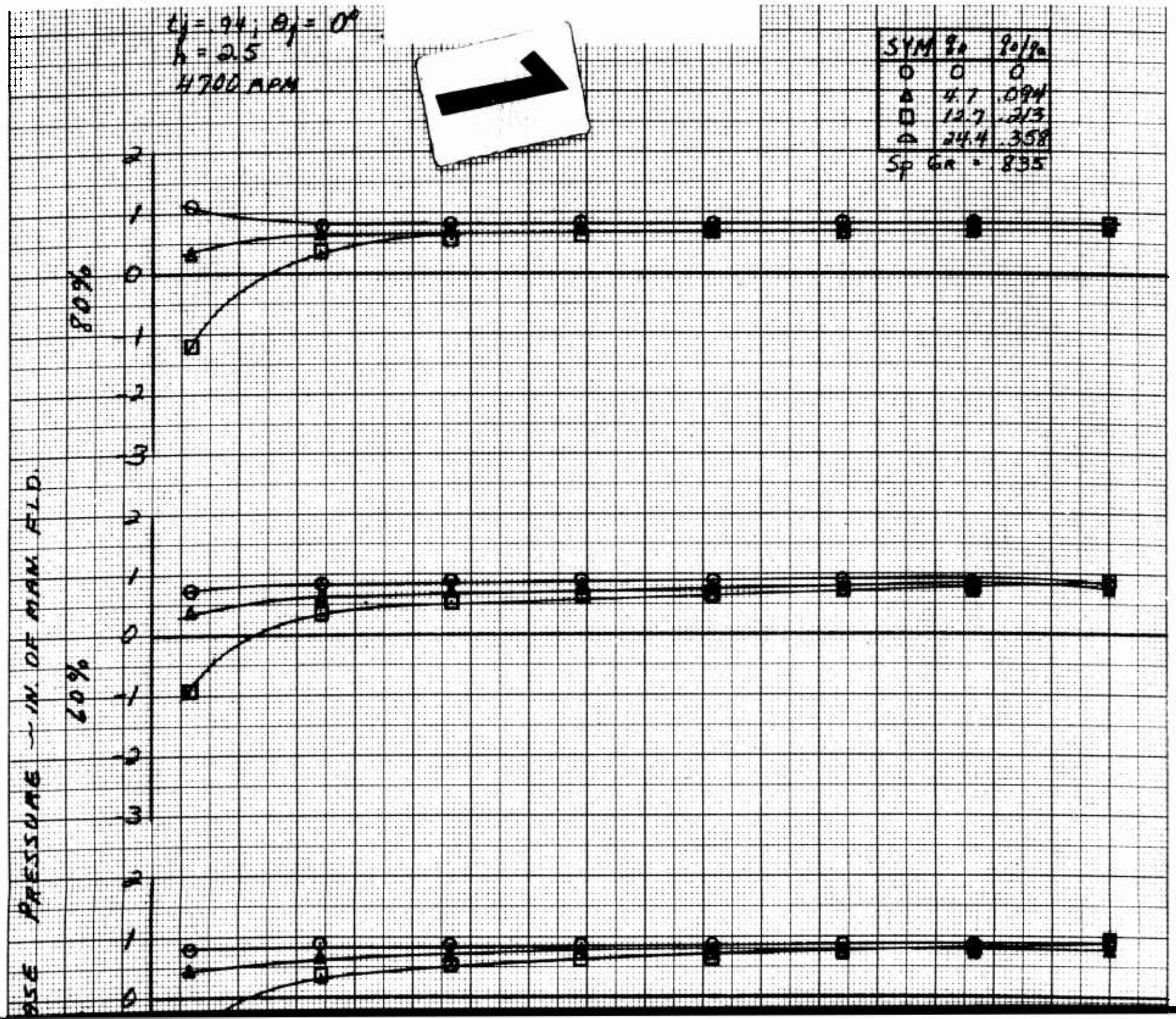
t_f = 94, θ_f = 0°
h = 2.5
4700 RPM
SYM | q_∞ | q_0/q_∞
○ | 0 | 0
△ | 4.7 | .094
□ | 12.7 | .213
◇ | 24.4 | .358
Sp Gr = .835
80%
60%
BASE PRESSURE — IN. OF MAN. FLD.

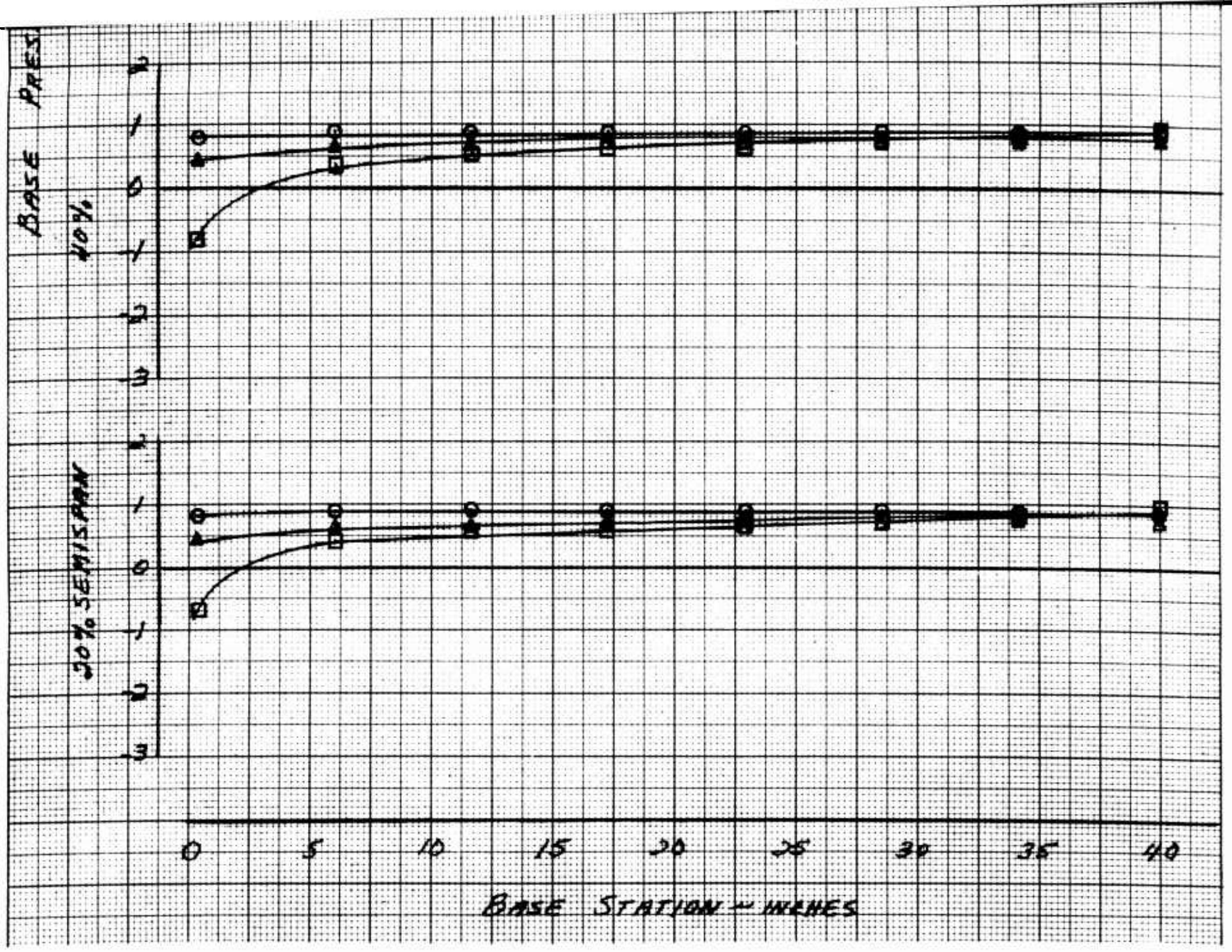

Fig. 17 Base Pressure Data, h = 2.5, t_j = .94, ϕ_j = 0, 4700 rpm

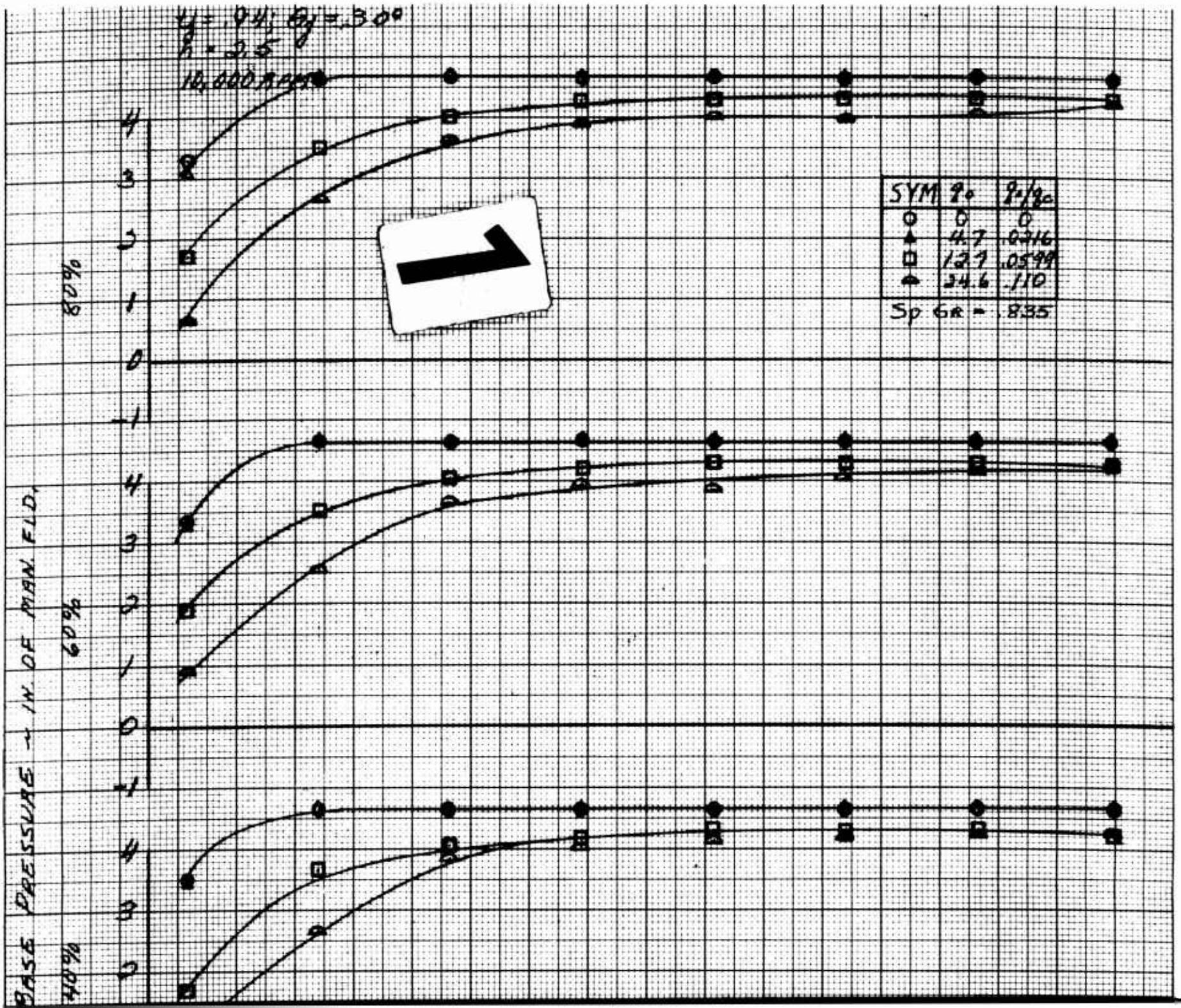
$\bar{y}$ = .04; $\bar{\theta}_y$ = 3.0°
$\bar{h}$ = 3.5"
16,000 RPM
SYM | q_o | q_o/q_c
○ | 0 | 0
▲ | 4.7 | .0216
□ | 12.1 | .0599
◆ | 24.6 | .110
Sp Gr = .835
80%
60%
40%
BASE PRESSURE - IN. OF MAN. FLD.

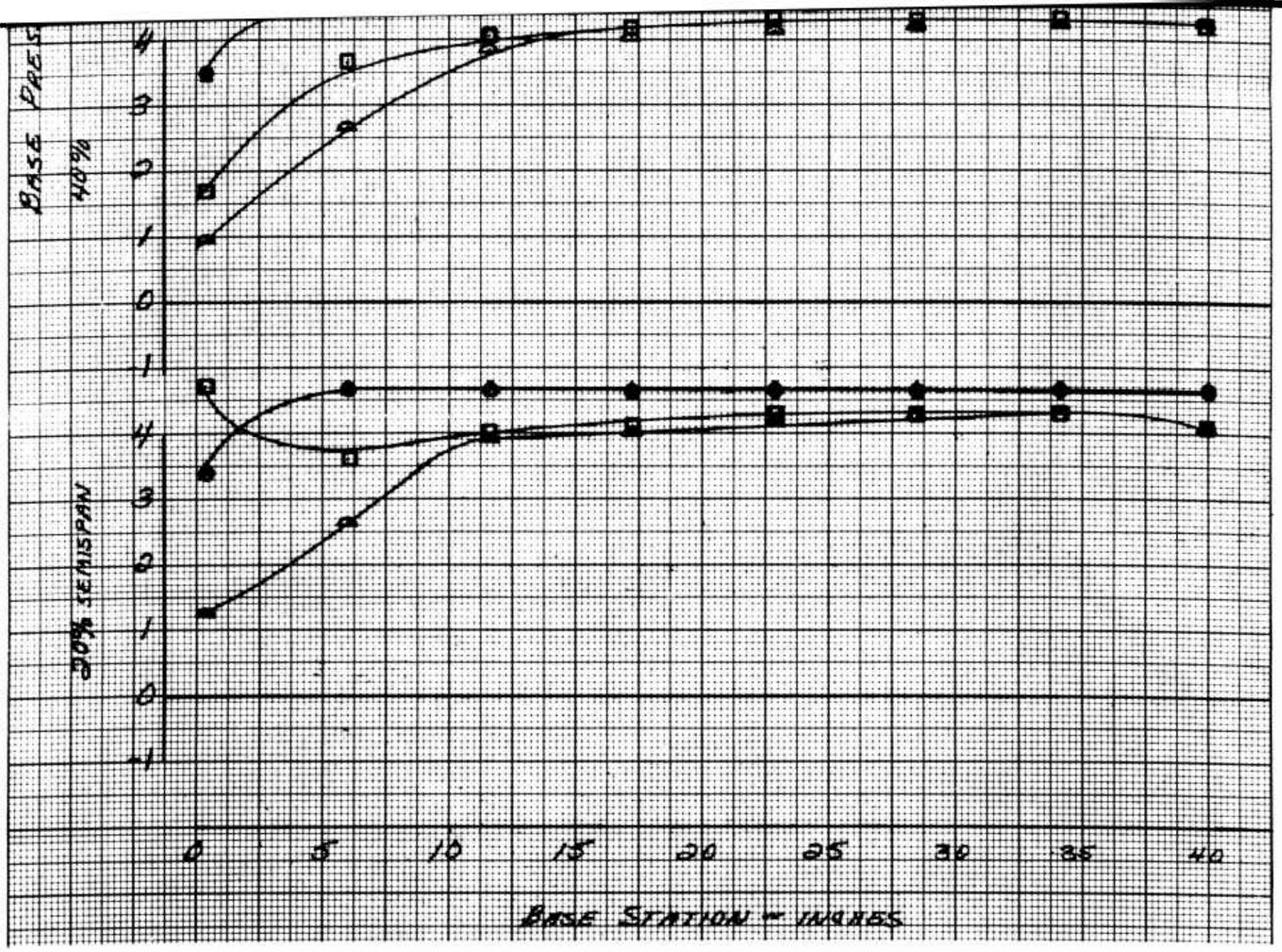

Fig. 18 Base Pressure Data, h = 2.5, t_j = .94, σ_j = 30, 10000 rpm

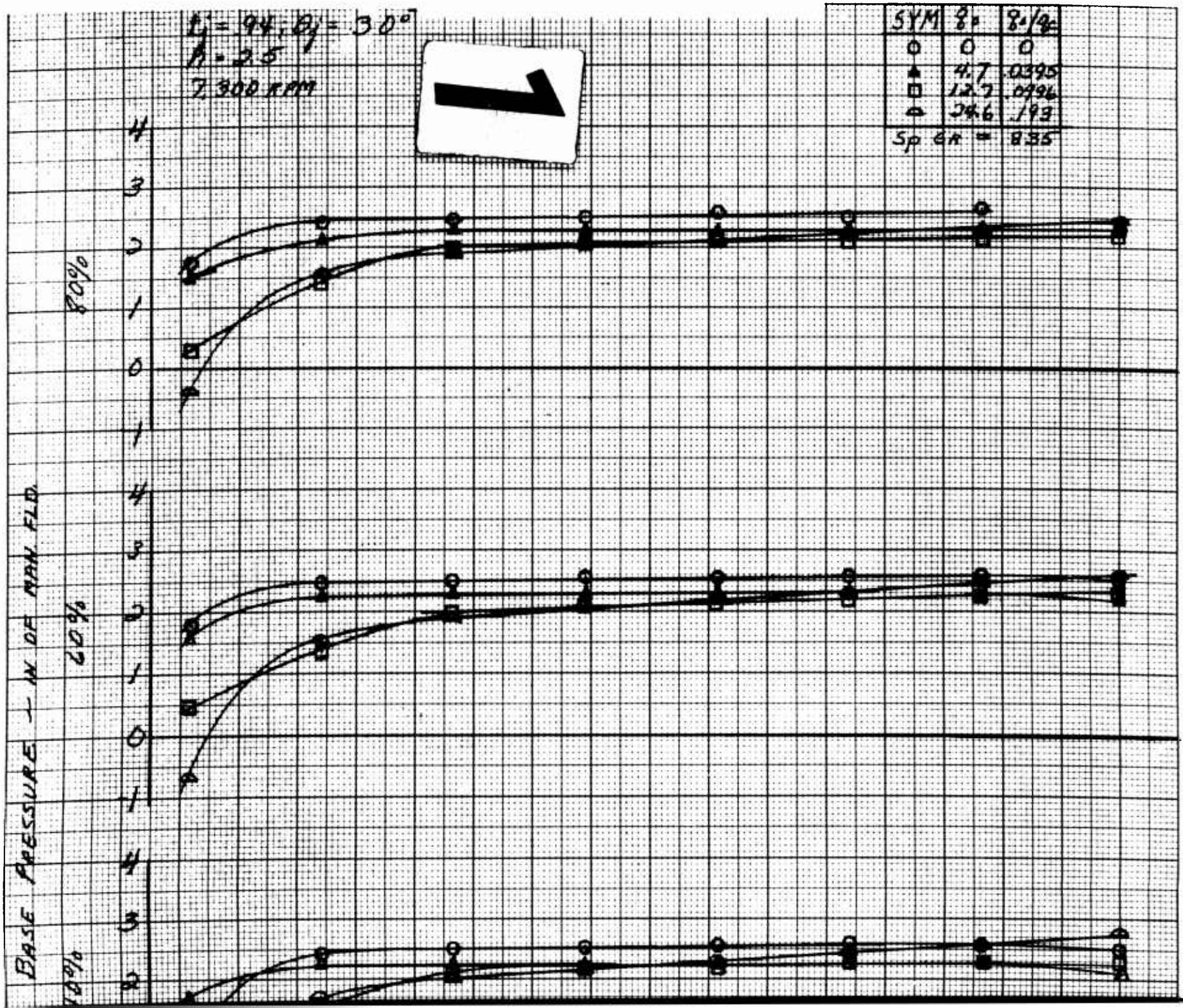
L_j = 94, θ_j = 30°
h = 2.5
7,300 RPM
7
SYM | δ_0 | δ_0/δ_c
0 | 0 | 0
▲ | 4.7 | .0395
□ | 12.7 | .0996
◇ | 24.6 | .193
Sp Gr = 8.35
80%
60%
40%
4
3
2
1
0
1
4
3
2
1
0
1
4
3
2
BASE PRESSURE + W OF MAN FLD

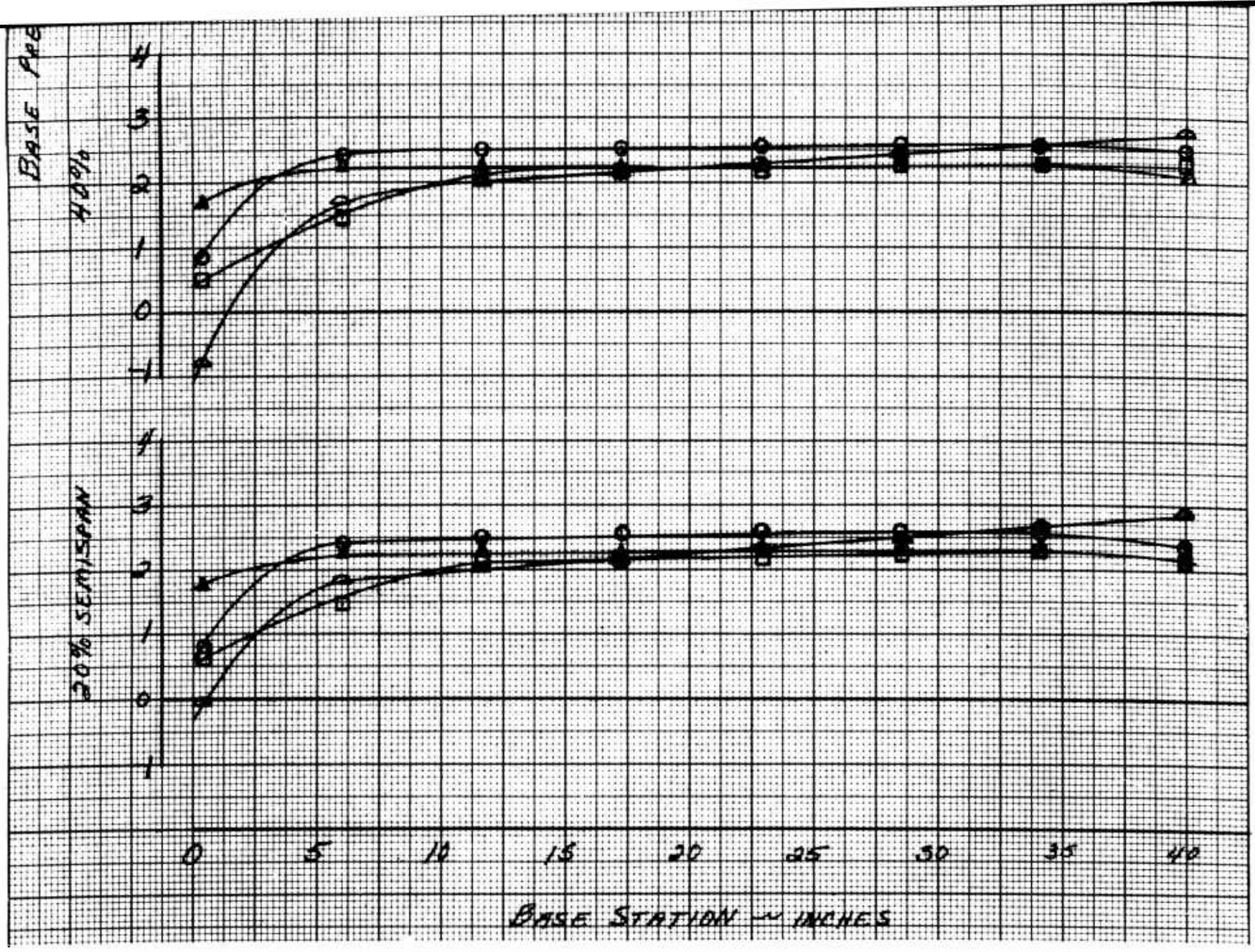

Fig. 19 Base Pressure Data, h = 2.5, t_j = .94, v_j = 30, 7300 rpm

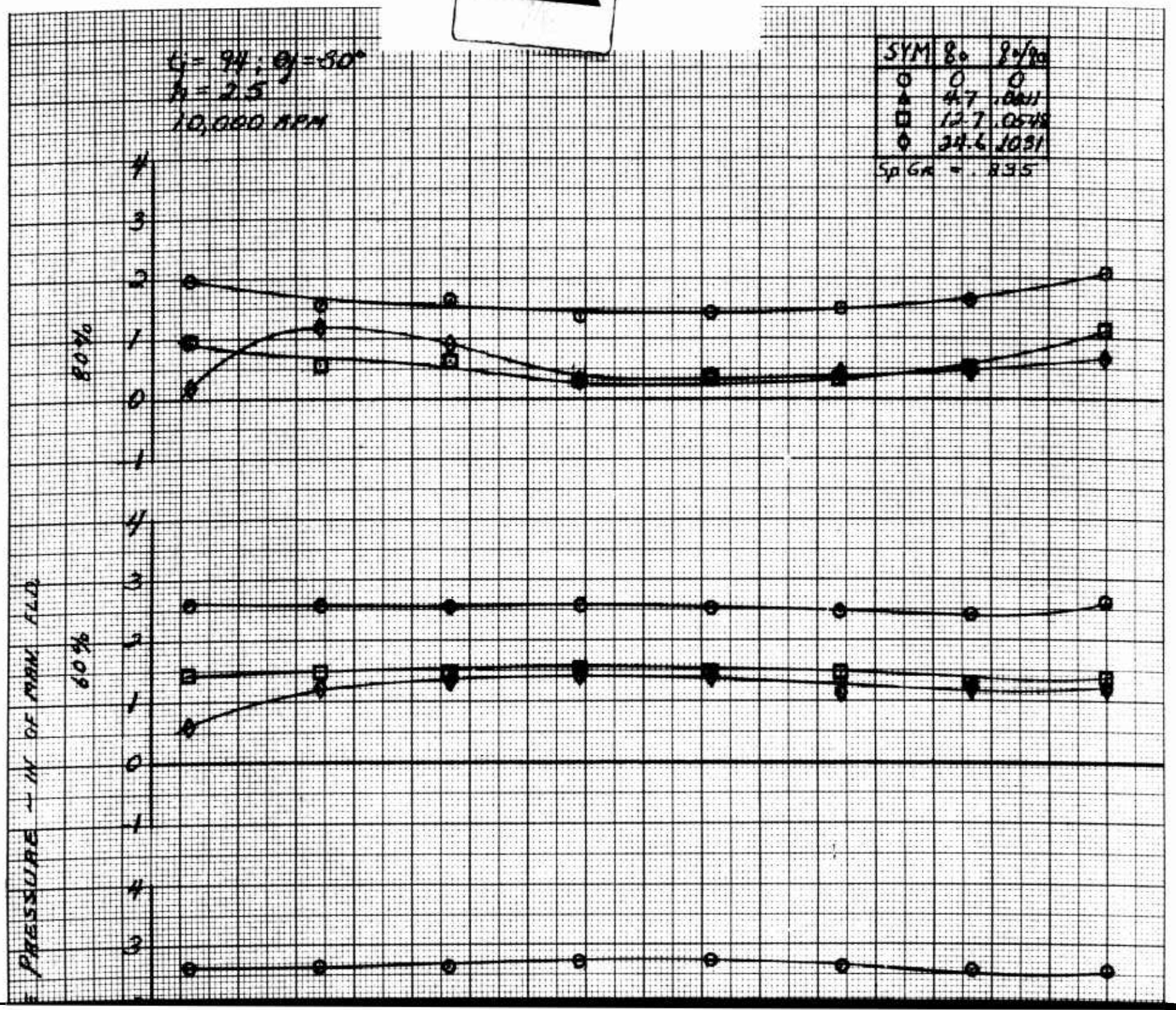
$C_J = .94$; $\theta_J = 30°$
$h = 2.5$
10,000 RPM
SYM | δ_0 | δ_0/δ_{0J}
0 | 0 | 0
▲ | 4.7 | .0811
□ | 12.7 | .0548
◆ | 24.4 | .1091
Sp Gr = .835
80%
60%
PRESSURE - IN. OF MAN. H2O

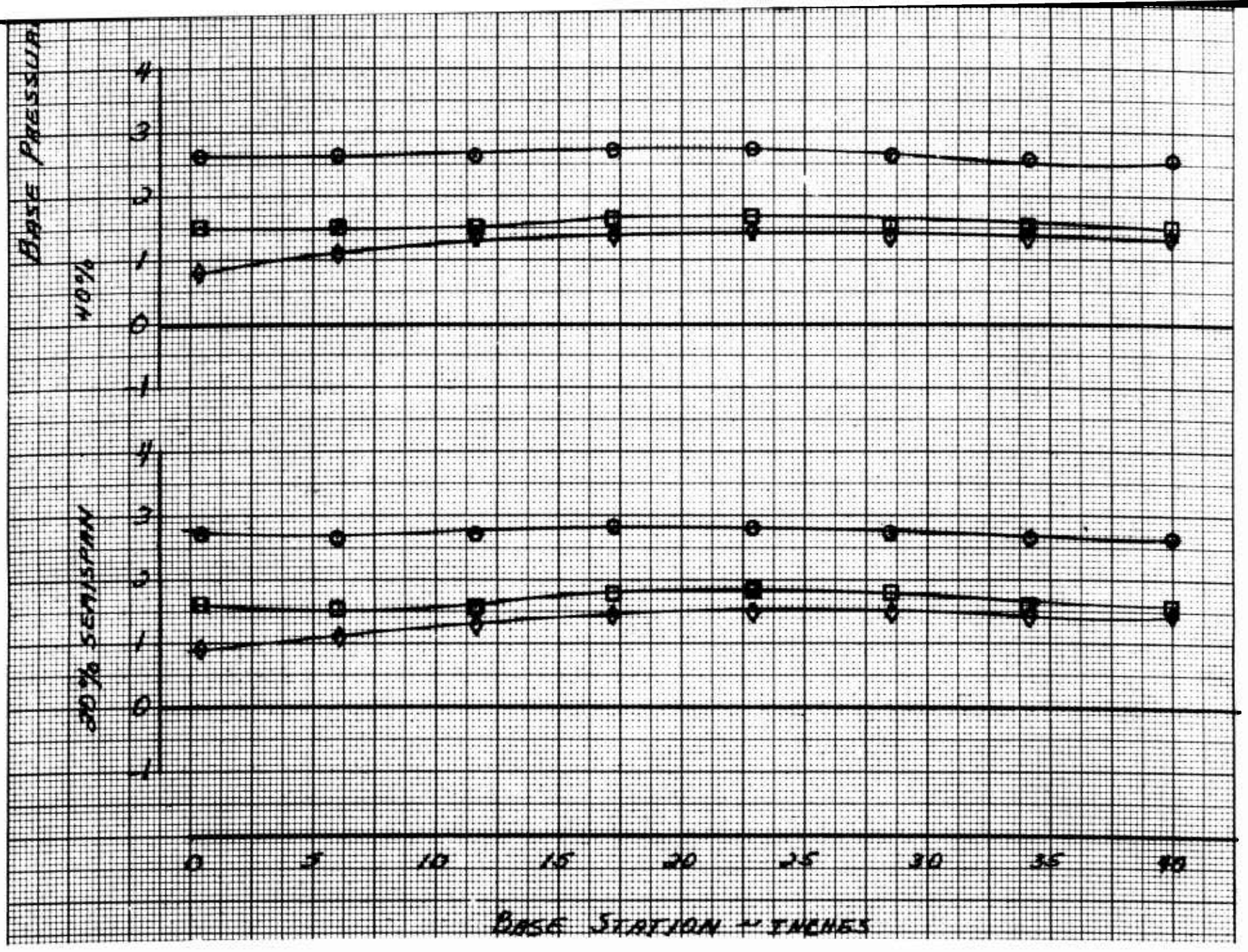

Fig. 20 Base Pressure Data, h = 2.5, t_j = .94, θ_j = -30, 10000 rpm

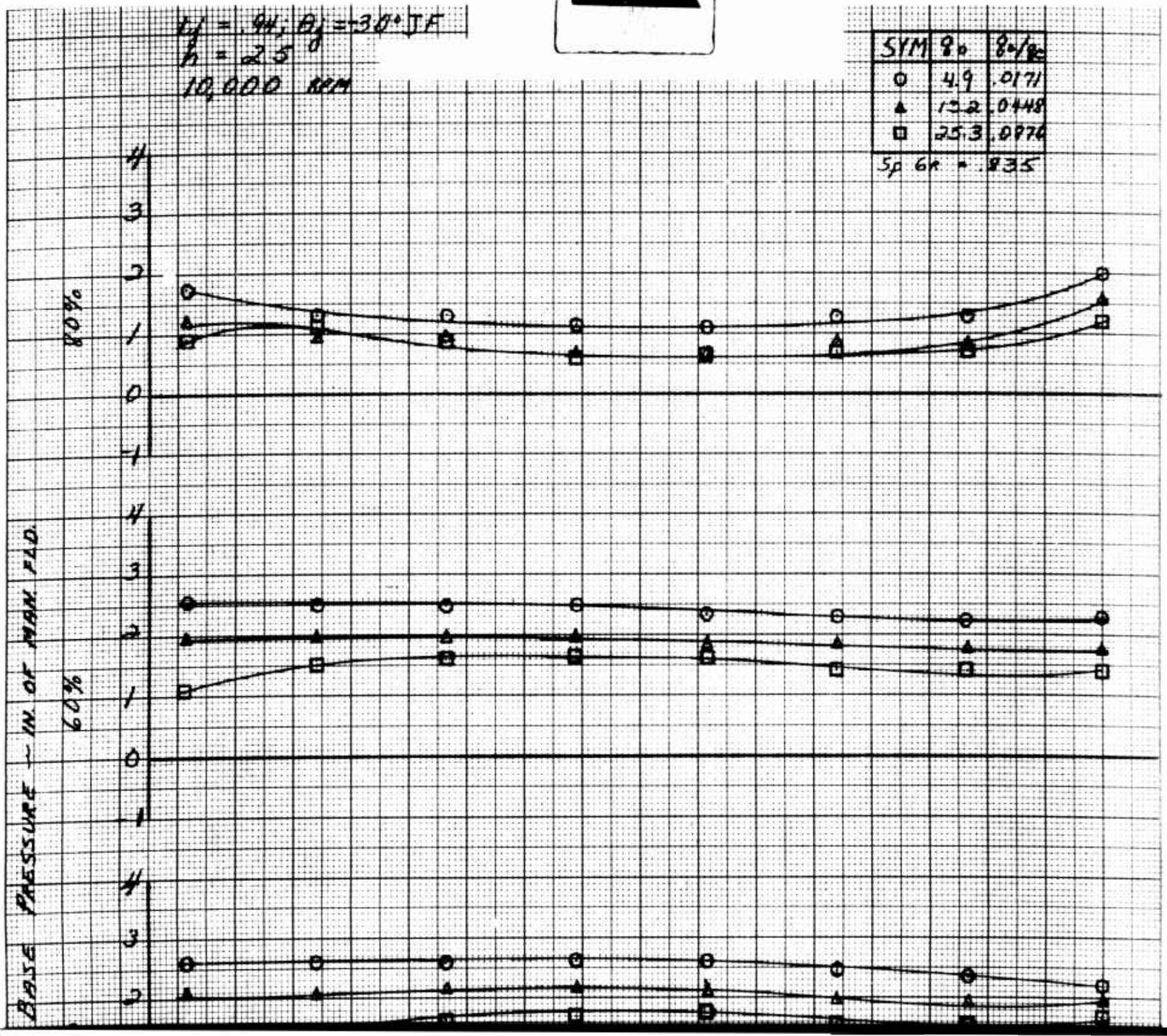
M_f = .94, θ_f = -30° TF
h = 25
10,000 RPM
SYM | q_0 | q_0/p_c
○ 4.9 .0171
▲ 12.2 .0448
□ 25.3 .0974
Sp 6K = .835
80%
60%
BASE PRESSURE - IN. OF MAN. H.D.

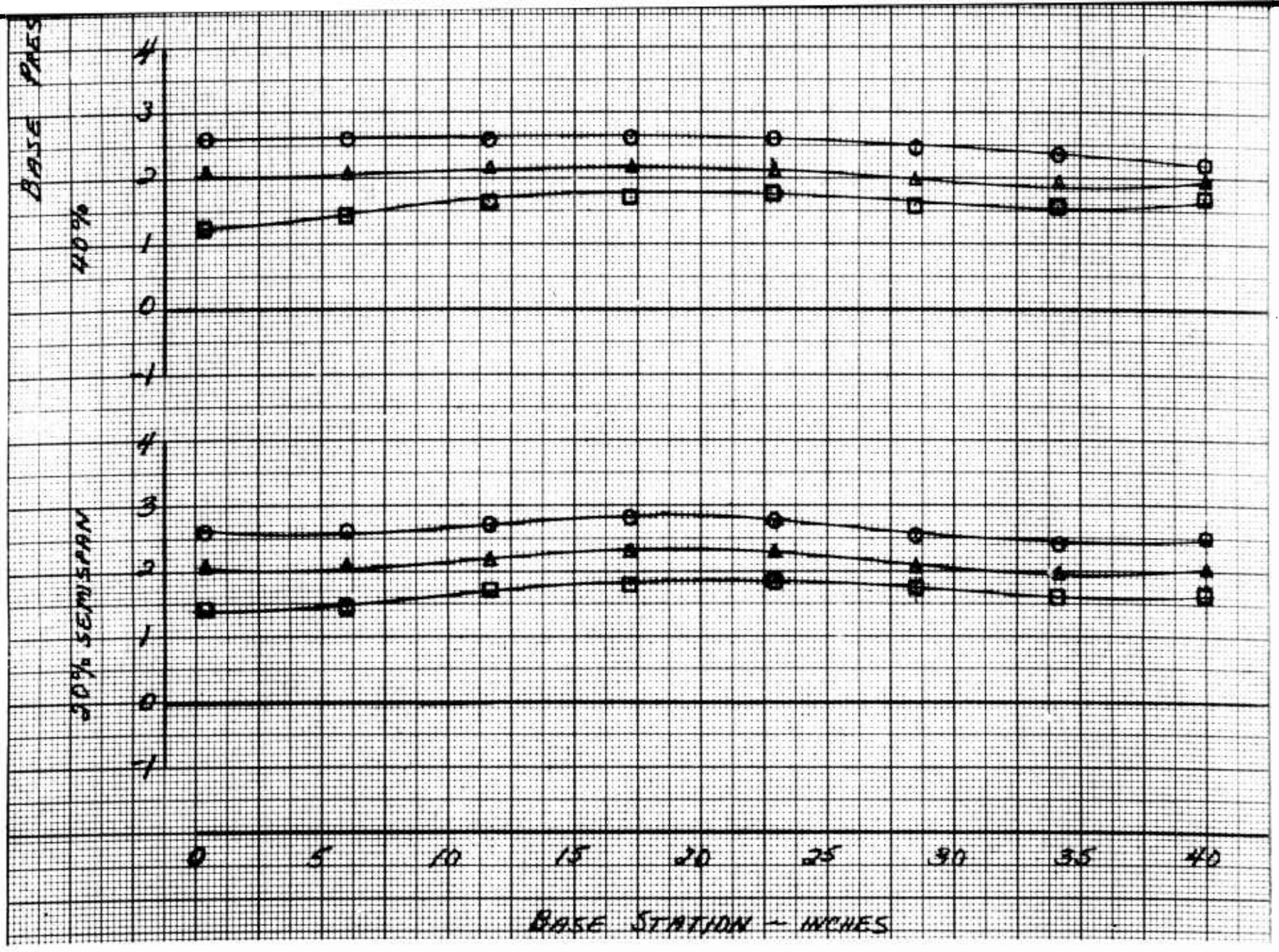

Fig. 21 Base Pressure Data, h = 2.5, t_j = .94, $_j$ = -30JF, 10000 rpm

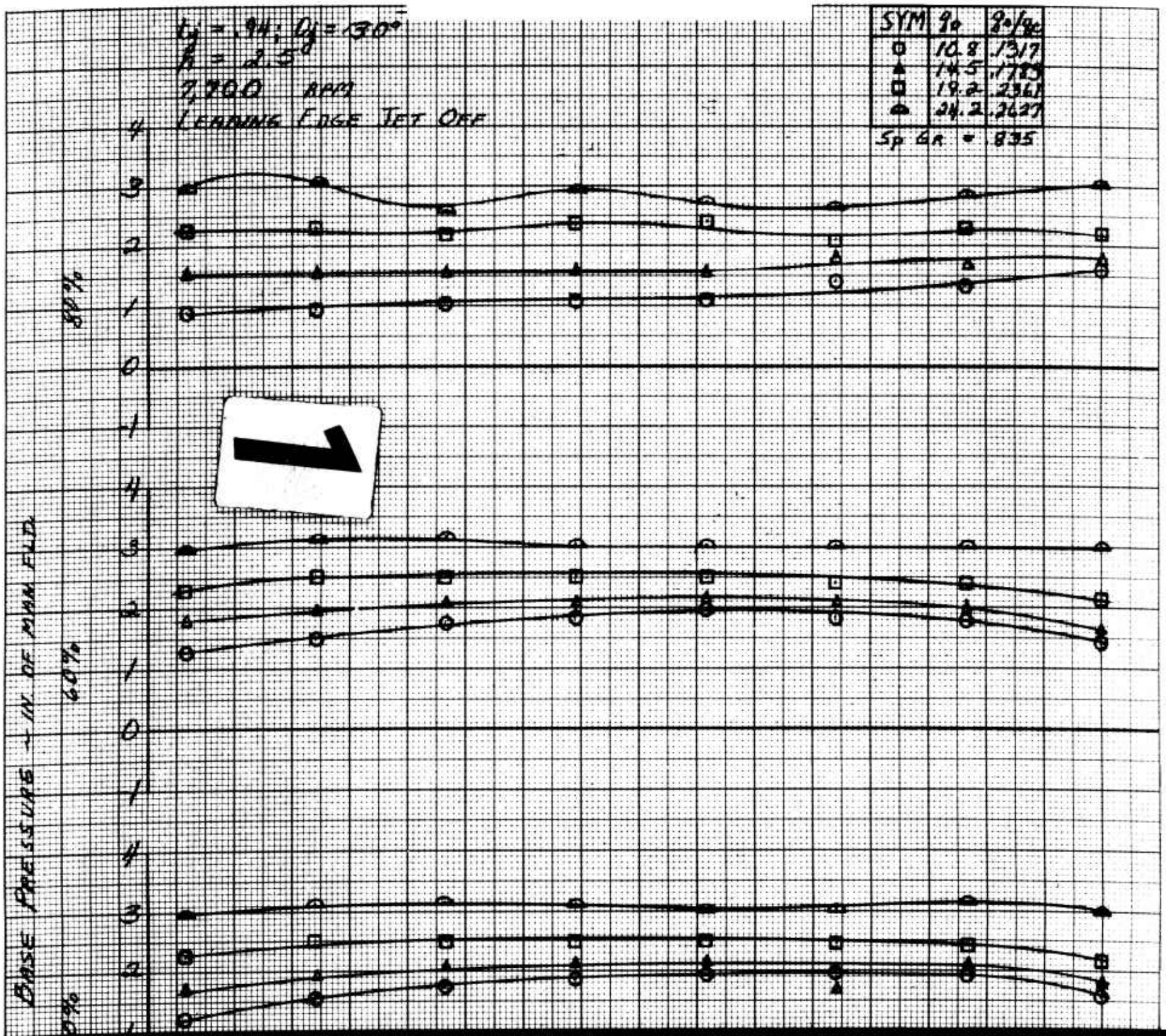
C_J = .94; θ_J = 30°
h = 2.5
7,700 RPM
LEADING EDGE JET OFF
SYM | q_0 | q_0/q_{sc}
10.8 | .1317
14.5 | .1783
19.2 | .2361
24.2 | .2977
Sp Gr = .835
BASE PRESSURE + IN. OF MAN FLD.
50%
60%
4
3
2
1
0
-1
-2
-3
-4

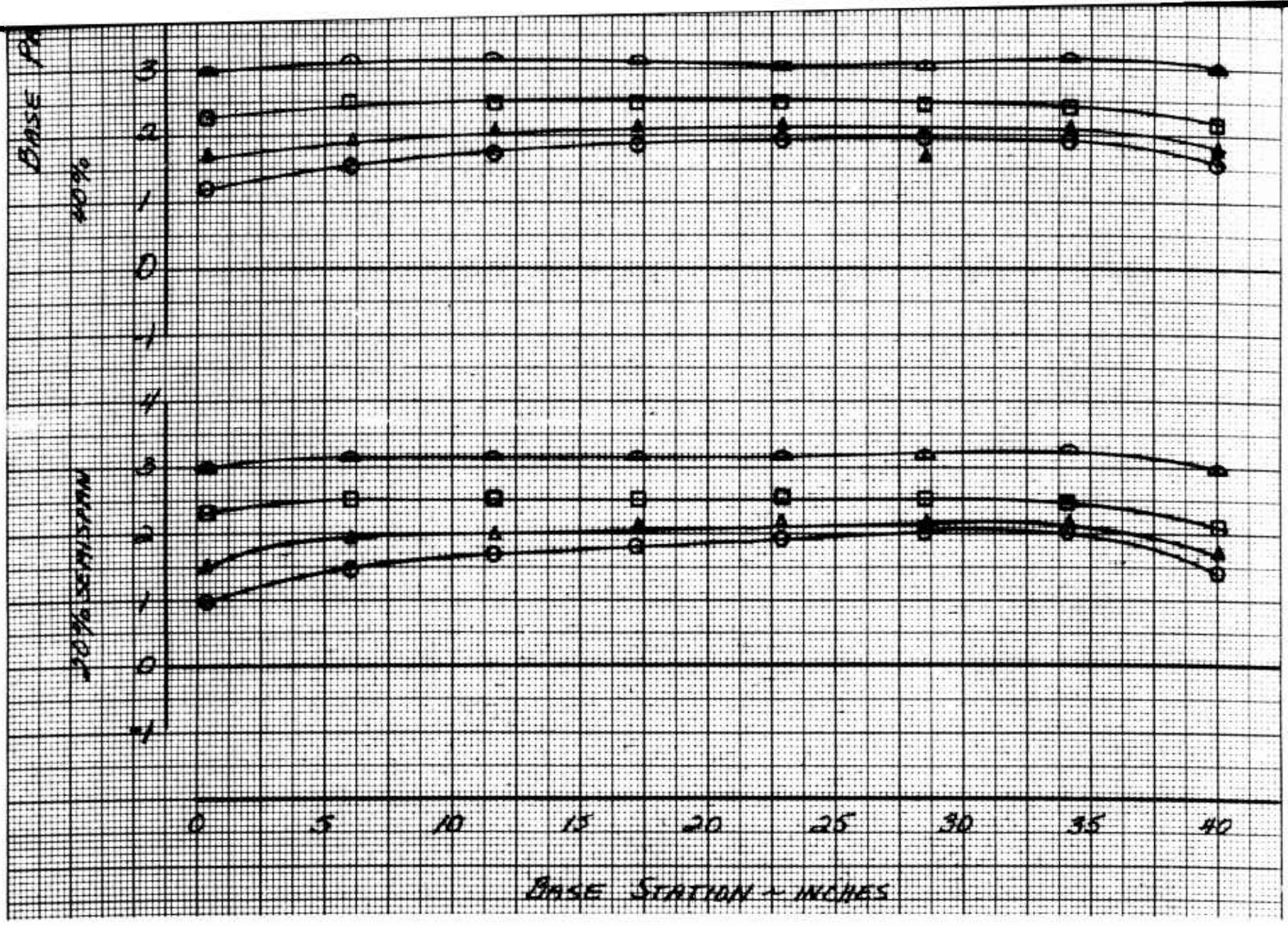

Fig. 22 Base Pressure Data, h = 2.5, t_j = .94, v_j = 30, 7700 rpm, Leading Edge Jet Off

$t_j = .94$; $\theta_j = 30°$
$\frac{t}{h} = .25$
7,700 RPM
LEADING EDGE JET OFF

SYM	p_o	p_o/p_c
○	10.8	.1528
△	14.5	.1769
□	19.2	.2078
◇	24.2	.2454

S_p GR = .935

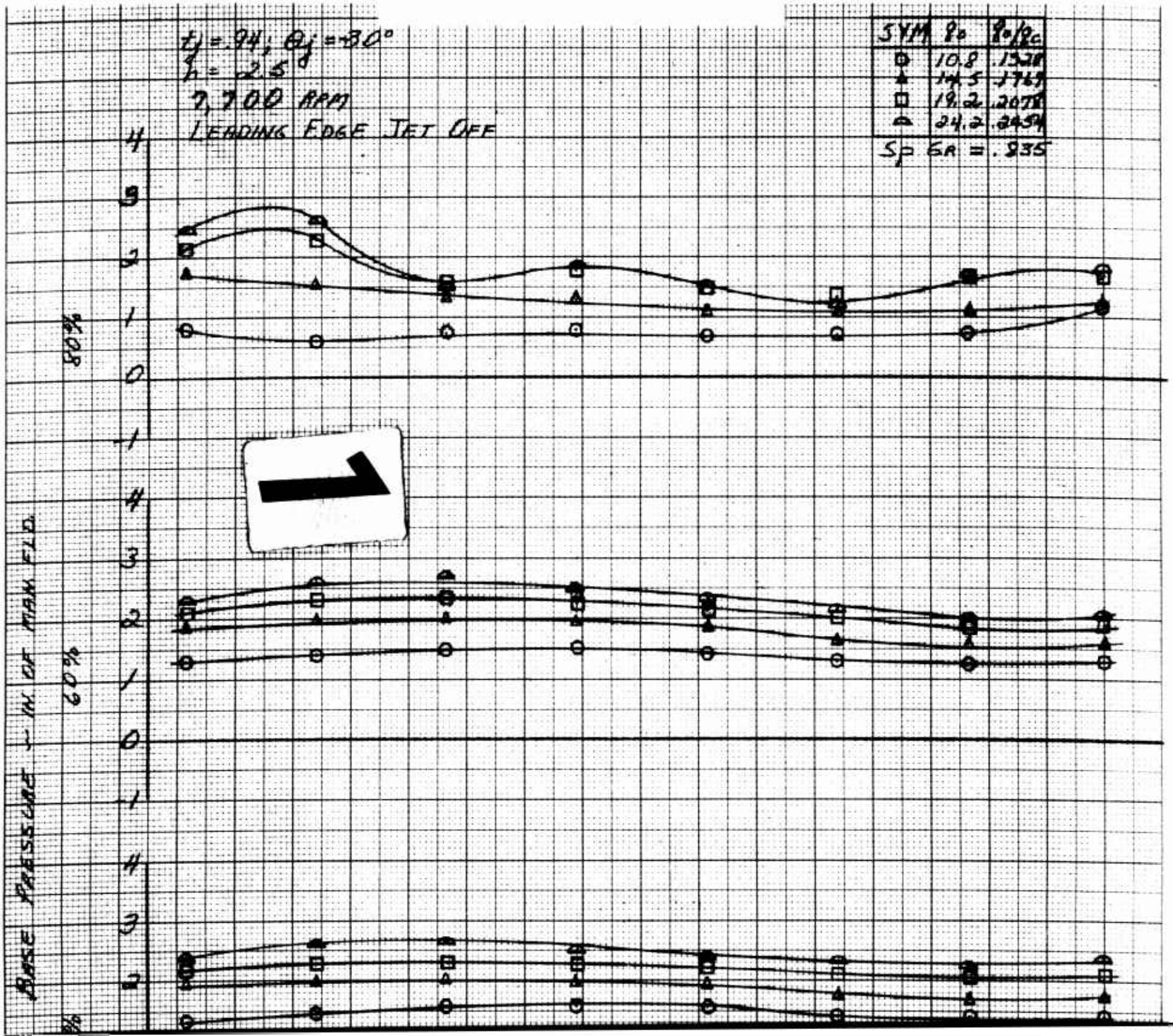

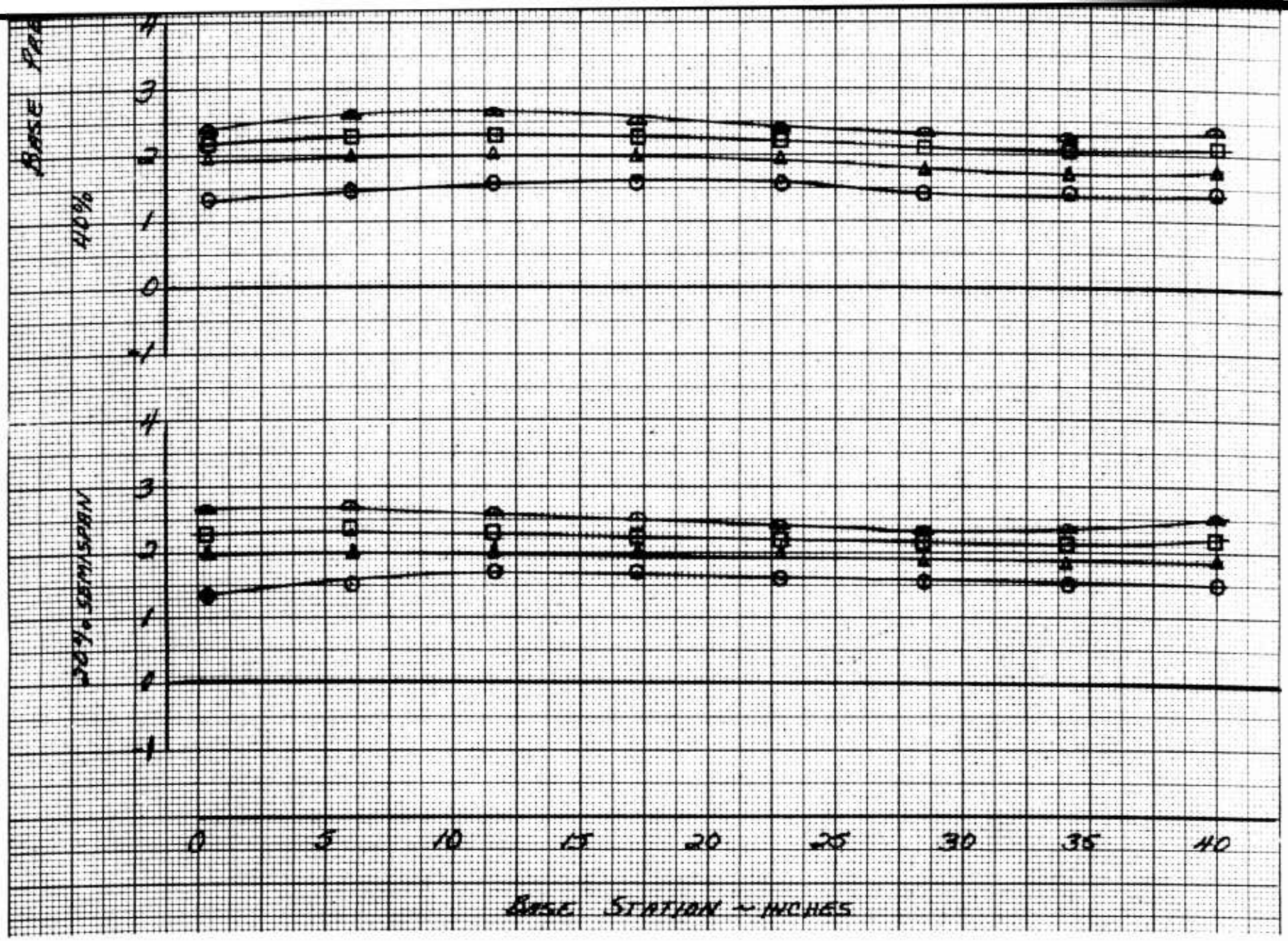

Fig. 23 Base Pressure Data, h = 2.5, t_j = .94, σ_j = -30, 7700 rpm
Leading Edge Jet Off

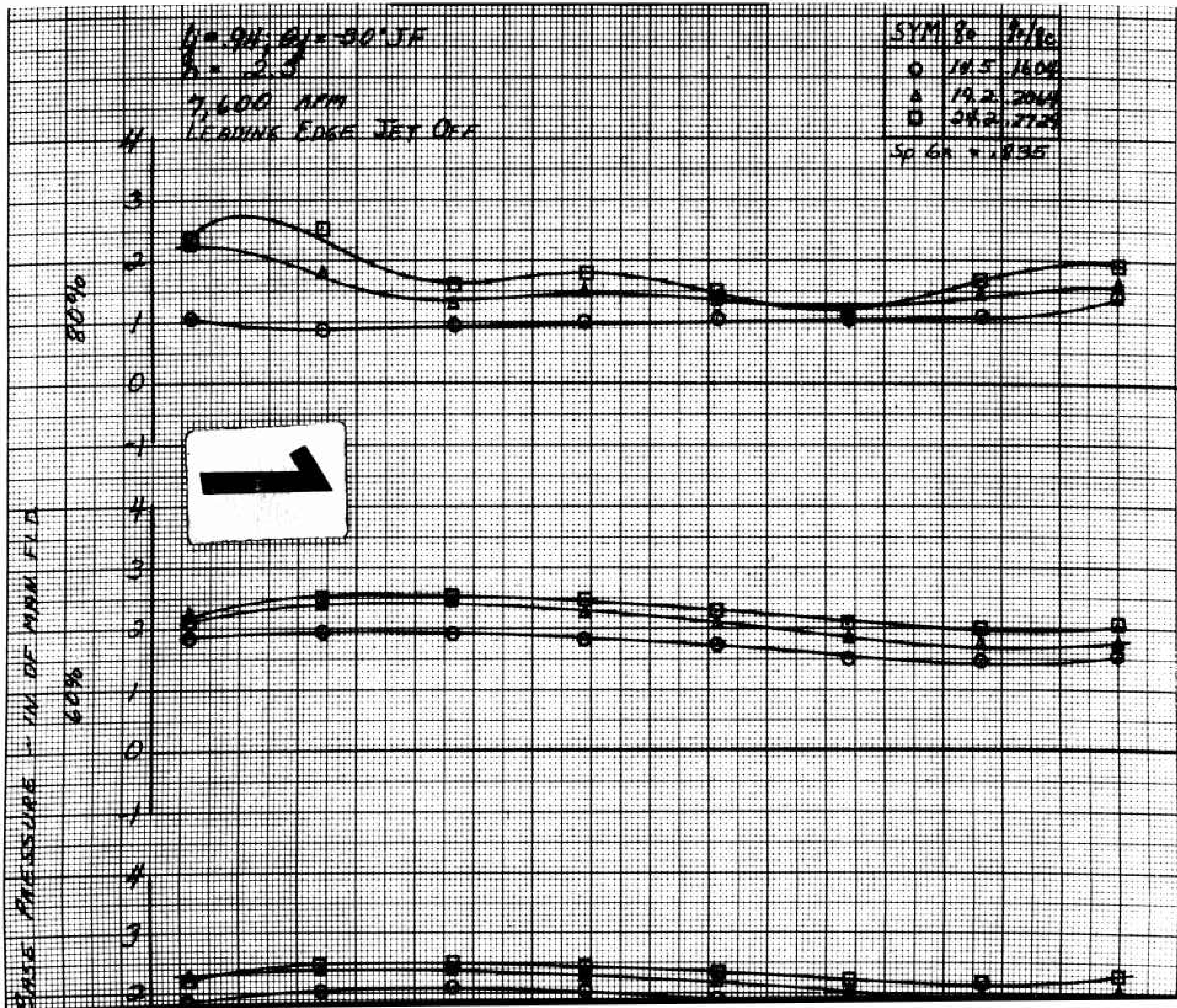

Cμ = .914; δf = 30° JF
h = 2.3
7,600 RPM
Leading Edge Jet Off
SYM
δ0
h/c
14.5
.1604
19.2
.2044
24.2
.2724
Sp Gr = .835
80%
60%
Base Pressure – in of Man Fld

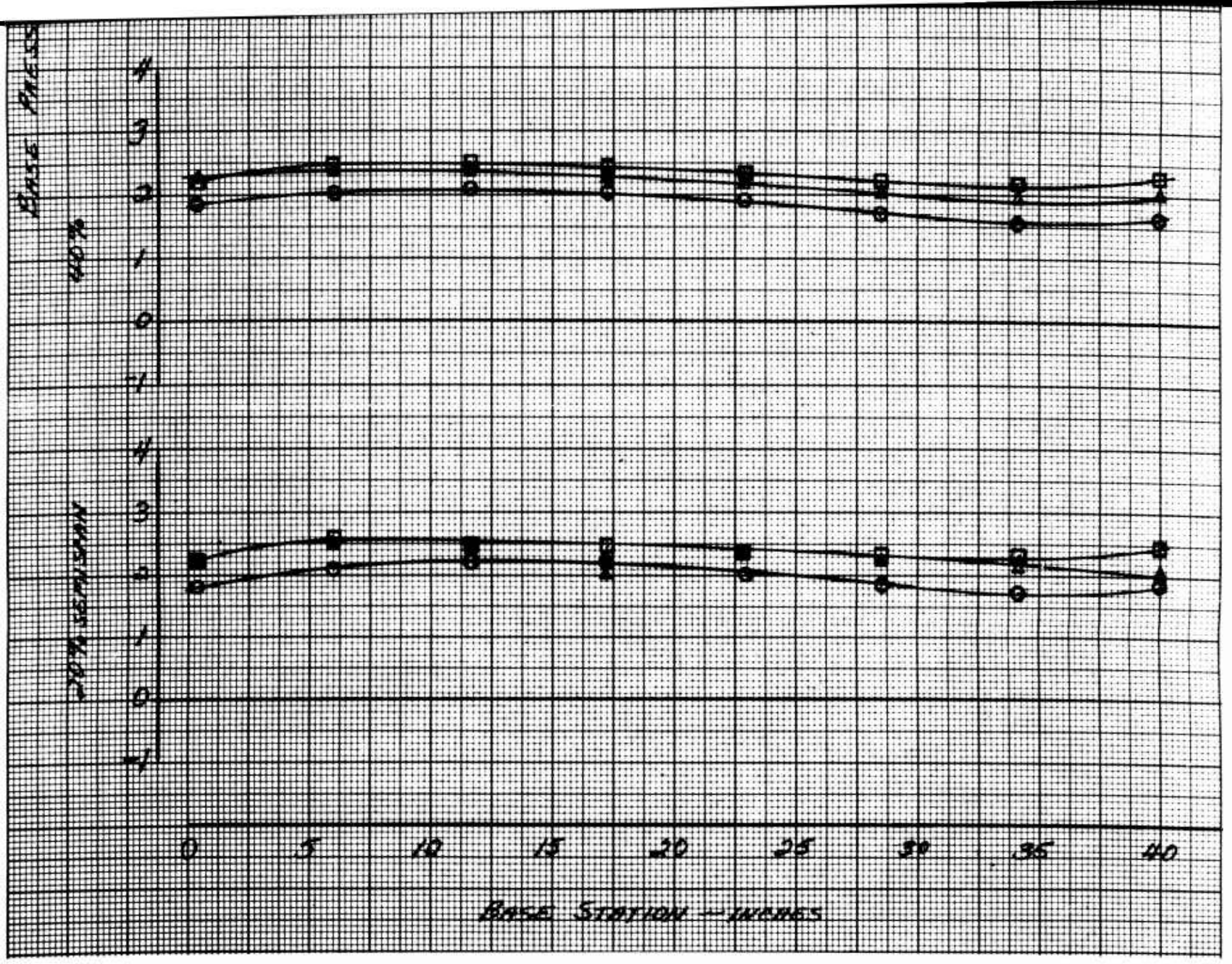

Fig. 24 Base Pressure Data, h = 2.5, t_j = .94, θ_j = -30JF, 7600 rpm, Leading Edge Jet Off

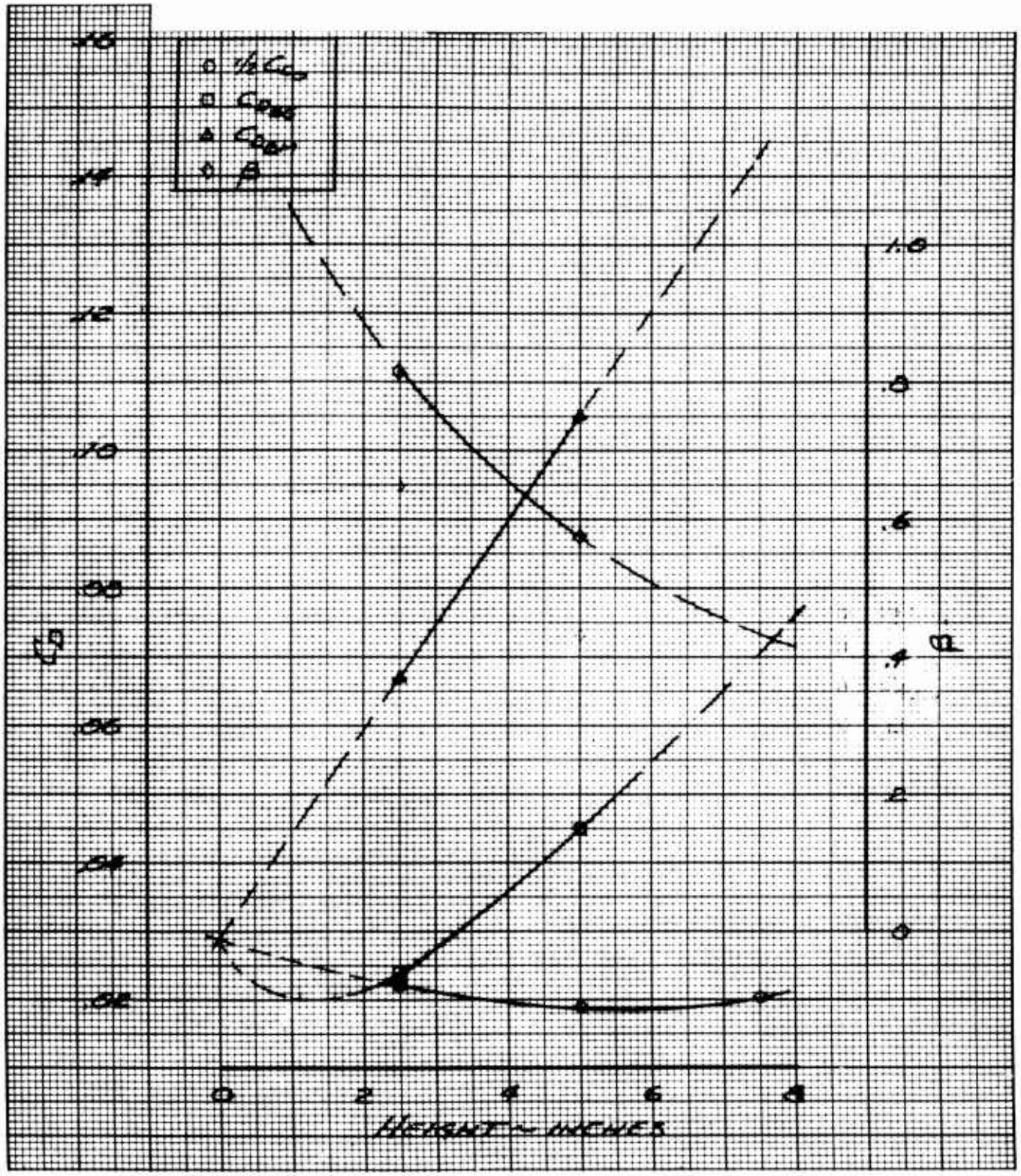

Fig. 25 Extrapolation of Mound Flow Data, Drag

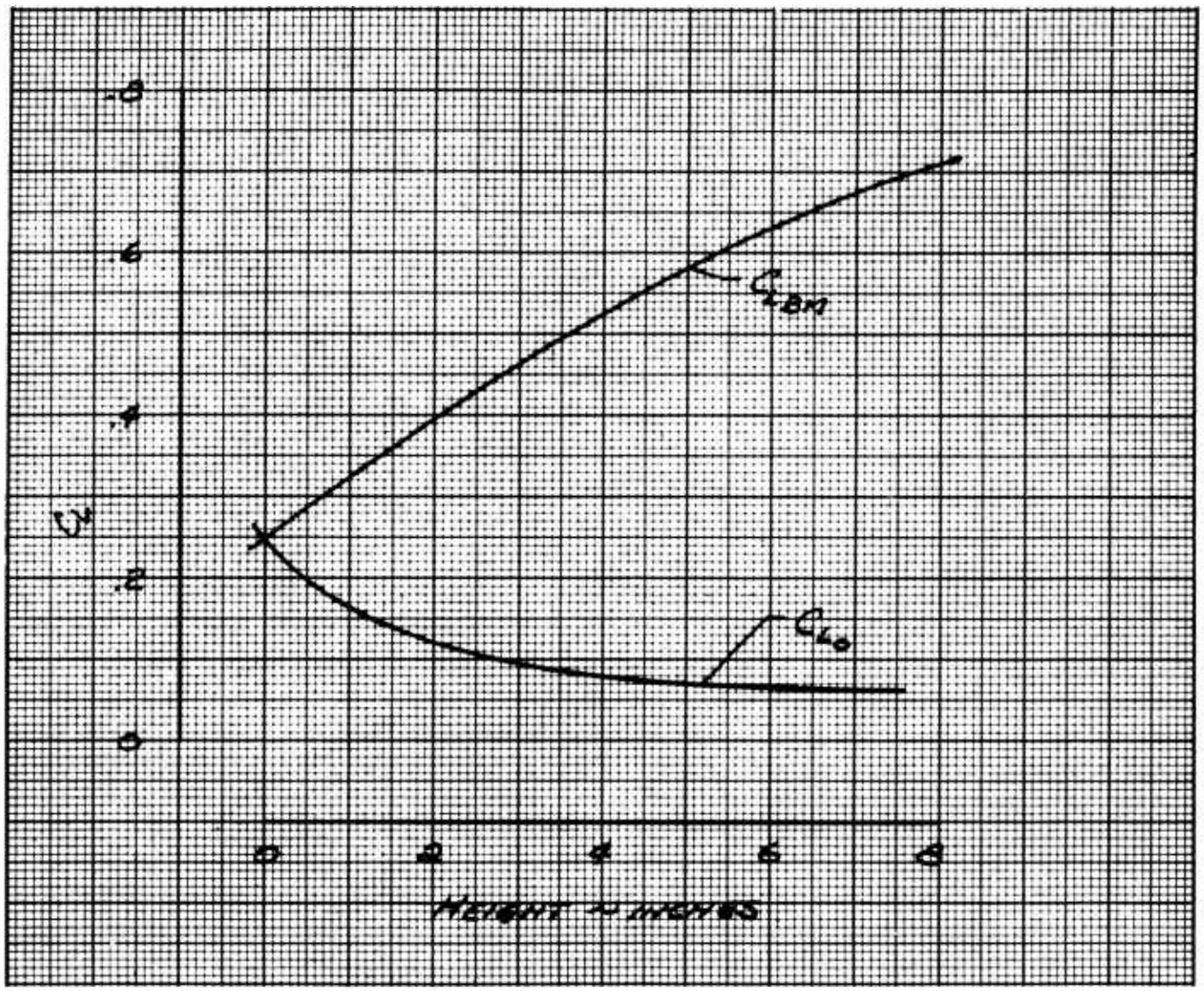

Fig. 26 Extrapolation of Mound Flow Data, Lift

UNCLASSIFIED